

Non-Abelian chiral soliton lattice in rotating QCD matter: Nambu-Goldstone and excited modes

Minoru Eto^{a,b} Kentaro Nishimura^{c,b} and Muneto Nitta^{d,b,c}

^a*Department of Physics, Yamagata University, Kojirakawa-machi 1-4-12, Yamagata, Yamagata 990-8560, Japan*

^b*Research and Education Center for Natural Sciences, Keio University, 4-1-1 Hiyoshi, Yokohama, Kanagawa 223-8521, Japan*

^c*International Institute for Sustainability with Knotted Chiral Meta Matter (SKCM²), Hiroshima University, 1-3-2 Kagamiyama, Higashi-Hiroshima, Hiroshima 739-8511, Japan*

^d*Department of Physics, Keio University, 4-1-1 Hiyoshi, Kanagawa 223-8521, Japan*

E-mail: meto@sci.kj.yamagata-u.ac.jp, nishiken@hiroshima-u.ac.jp, nitta@phys-h.keio.ac.jp

ABSTRACT: The ground state of QCD with two flavors at a finite baryon chemical potential under rapid rotation is a chiral soliton lattice (CSL) of the η meson, consisting of a stack of sine-Gordon solitons carrying a baryon number, due to the anomalous coupling of the η meson to the rotation. In a large parameter region, the ground state becomes a non-Abelian CSL, in which due to the neutral pion condensation each η soliton decays into a pair of non-Abelian sine-Gordon solitons carrying S^2 moduli originated from Nambu-Goldstone (NG) modes localized around it, corresponding to the spontaneously broken vector symmetry $SU(2)_V$. There, the S^2 modes of neighboring solitons are anti-aligned, and these modes should propagate in the transverse direction of the lattice due to the interaction between the S^2 modes of neighboring solitons. In this paper, we calculate excitations including gapless NG modes and excited modes around non-Abelian and Abelian (η) CSLs, and find three gapless NG modes with linear dispersion relations (type-A NG modes): two isospinons (S^2 modes) and a phonon corresponding to the spontaneously broken vector $SU(2)_V$ and translational symmetries around the non-Abelian CSL, respectively, and only a phonon for the Abelian CSL because of the recovering $SU(2)_V$. We also find in the deconfined phase that the dispersion relation of the isospinons becomes of the Dirac type, *i. e.* linear even at large momentum.

Contents

1	Introduction	1
2	Non-Abelian chiral soliton lattices	4
2.1	General setup	4
2.2	The noninteractive case of $\epsilon = 0$ and $\beta = 0$	7
2.3	Confined phase	8
2.4	Deconfined phase	9
2.5	Dimer phase	9
3	Dispersion relations around chiral soliton lattices	9
3.1	Equations of motion for fluctuations	10
3.1.1	The neutral components: phonons	11
3.1.2	The charged components: isospinons	14
3.2	The noninteractive case of $\epsilon = 0$ and $\beta = 0$	16
3.3	Confined phase	22
3.4	Deconfined phase	22
3.5	Dimer phase	24
4	Summary and discussion	25

1 Introduction

The strong interaction, one of the fundamental forces, can be described by quantum chromodynamics (QCD), the theory for quarks and gluons. In the vacuum, one does not observe quarks, but there are only hadrons, *i. e.* baryons made of three quark-bound states and mesons made of quark–anti-quark bound states. In fact, a lattice formulation of QCD can show such quark confinement at the quantitative level. However, because of the sign problem, the lattice QCD cannot describe a situation at finite baryon density relevant for neutron star interiors and heavy-ion colliders. In order to explore such a situation, much attention has been paid to QCD phase diagram at finite baryon density under external fields such as strong magnetic field and rapid rotation [1].

Low-energy dynamics of QCD can be described in terms of Nambu-Goldstone(NG) bosons, that is pions, when the chiral symmetry is spontaneously broken. Theoretically, it is a chiral Lagrangian or the chiral perturbation theory (ChPT), which is unique up to some constants, the pion’s decay constant, quark masses, and so on [2, 3]. In the presence of an external magnetic field, the chiral Lagrangian is accompanied by the anomalous coupling of the neutral pion π_0 to the magnetic field via the chiral anomaly [4, 5] through the Goldstone-Wilczek current [6, 7]. Then, the ground state of QCD with two flavors (up and

down quarks) at a finite baryon chemical potential in the presence of a sufficiently strong magnetic field was found to be a chiral soliton lattice (CSL) consisting of a stack of domain walls or sine-Gordon solitons carrying a baryon number [5, 8, 9].¹ However, such a CSL is unstable against a charged pion condensation in a region of higher density and/or stronger magnetic field [12]. One of the possibilities for the fate of the instability is an Abrikosov's vortex lattice or baryon crystal [13, 14]. On the other hand, we showed in refs. [15, 16] that there appears to be a lower energy state before going to such an unstable region, *i. e.* the domain-wall Skyrmion phase in which Skyrmons are created on top of the solitons in the ground state. The instability of the CSL is present in the region where it is metastable and the ground state is the domain-wall Skyrmion phase [16]. Possible relations between Skyrmion crystals in the absence of the magnetic field and the CSL phase were discussed in refs. [17–19]. The other topics of the CSLs include, for instance CSLs under thermal fluctuation [12, 20–22], quantum nucleation of CSLs [23, 24], and quasicrystals [25].

Here, we concentrate on another important axis, rotation, in the phase diagram of QCD. Quark-gluon plasmas produced in non-central heavy-ion collision experiments at the Relativistic Heavy Ion Collider (RHIC) reach the largest vorticity observed thus far, of the order of $10^{22}/\text{s}$ [26, 27]. This has triggered significant attention to rotating QCD matter in recent years [28–42]. In parallel to the case of a strong magnetic field, the CSL phase in rotating QCD matter was studied in refs. [39–43]: a contribution of the chiral anomaly to the η' meson was obtained by matching with the chiral vortical effect (CVE) [44–49] in terms of mesons [39, 40]. Due to the anomalous term, the ground state in a certain parameter region was found to be another type of CSL made of the η' meson [39, 40] instead of that of the neutral pion π_0 in the magnetic field. While in ref. [40] the pion fields are set to be zero, it cannot be justified always. In fact, it was found in ref. [42] that in a large parameter region in the two-flavor case² the neutral pion condensation occurs in the CSL to turn it a *non-Abelian CSL*, where a single η soliton decays into a pair of non-Abelian sine-Gordon solitons. For a single non-Abelian soliton, the η meson changes from 0 to π and the neutral pion π_0 changes from 0 to π so that the $U(2)$ group element is single-valued in the periodic boundaries, in contrast to a single η soliton for which only the η meson changes from 0 to 2π while the pions are zero. Because of a nontrivial π_0 profile, the vector symmetry $SU(2)_V$ unbroken in the vacuum is further broken spontaneously into a $U(1)$ subgroup in the vicinity of the soliton, resulting in $\mathbb{C}P^1[\simeq SU(2)/U(1)]$ NG modes localized around each soliton, thus dubbed a non-Abelian sine-Gordon soliton [50, 51] (see also refs. [52–54] for further study). The $\mathbb{C}P^1$ modes at two neighboring solitons repel each other, and thus they are antialigned. Thus, if one calls one soliton an up-soliton, then its neighboring solitons can be called down-solitons, and the up and down solitons appear alternately in the whole lattice. Thus, non-Abelian CSL can be regarded as a Heisenberg anti-ferromagnetic spin

¹It is known that some inhomogeneous states modulated along one direction are unstable under transverse fluctuations assuming the $SO(3)$ rotational symmetry of the system, which is called the Landau-Peierls instability [10, 11]. However, in this case, such an instability is absent because the $SO(3)$ rotational symmetry is explicitly broken by magnetic field or rotation.

²In the two-flavor case, the η meson plays a role in constituting a CSL instead of the η' meson in the three-flavor case.

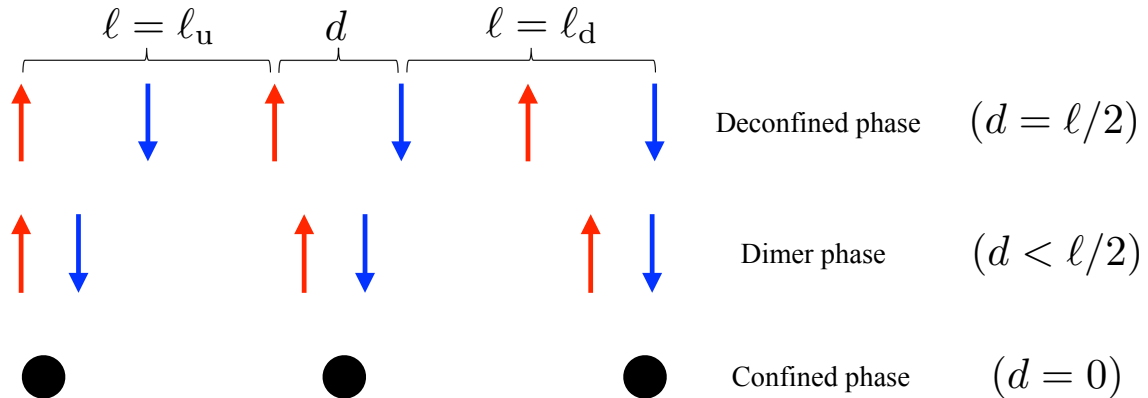


Figure 1. Schematic picture of an arrangement of the up (red arrow) and down (blue arrow) solitons. Since $l_+ = l_-$, the state where the up and down solitons farthest apart satisfies $d = \ell/2$. This state is called the deconfined phase. On the other hand, the state where the up and down solitons are completely overlapped (the black circle in this picture) is called the confined phase. The intermediate state satisfies $d < \ell/2$.

chain. Such a non-Abelian CSL can be distinguished by a \mathbb{Z}_2 symmetry into the two classes: the deconfined and dimer phases. In the deconfined phase, an up-soliton and down-soliton repel each other in real space, and thus up and down solitons appear alternately with the same distances, as illustrated in the upper line in fig. 1. In the dimer phase, they attract each other at large distances and repel at short distances, and thus constitute a molecule as illustrated in the middle line in fig. 1. In the confined phase, the up-soliton and down-soliton attract in the whole separation, and they completely overlap to constitute an η soliton, as illustrated in the bottom line in fig. 1. This is nothing but the η CSL, which is also called an Abelian CSL. These three phases appear in the phase diagram spanned by the ratio between the decay constants of the η meson and pions and the ratio between the anomaly coefficient and pion mass [42]. Furthermore, as in the case of the strong magnetic field, a domain-wall Skyrmion phase appears in a larger chemical potential region inside the non-Abelian CSL [43].

In this paper, we study excitations including gapless NG modes and massive modes around the three phases of CSLs mentioned above, the confined, deconfined and dimer phases. We also consider a noninteractive case, for which up and down solitons do not interact, and consequently, up solitons form a lattice, and down solitons form another lattice independently. In the classification of NG modes, type-A(B) NG modes correspond to the same number (a half) of broken generators, typically having linear (quadratic) dispersion relations [55–58], see refs. [59, 60] for a review. For example, magnons in (anti-)ferromagnets are type-B(A) NG modes with quadratic (linear) dispersion relations. Another example of NG modes in a soliton lattice is a phonon-like excitation propagating in transverse directions of a vortex lattice, called a Tkachenko mode [61–64], which is a type-B NG mode [65]. In the case of a non-Abelian CSL, non-Abelian solitons form a lattice, in which the $\mathbb{C}P^1$ modes of a pair of neighboring solitons are anti-aligned, and the $\mathbb{C}P^1$ modes as well as a phonon should be able to propagate in the transverse direction of the

lattice. Therefore, we work out fluctuations around the non-Abelian and Abelian CSLs and find three gapless NG modes with linear dispersion relations (type-A): two isospinons (the $\mathbb{C}P^1$ modes) corresponding to the spontaneously broken $SU(2)_V$ symmetry, beside a phonon corresponding to the spontaneously broken translational symmetry. In particular, the dispersion relation of the isospinons is of the Dirac type, *i. e.* linear even at large momentum in the deconfined phase, and is not so in the dimer phase. On the other hand, in the confined phase, we find only one gapless NG mode (a phonon) as expected, since the vector symmetry $SU(2)_V$ is not broken.

This paper is organized as follows. In sec. 2 we summarize non-Abelian CSLs. In sec. 3, we study fluctuations around the CSLs to obtain dispersion relations of NG modes and excited modes. Sec. 4 is devoted to a summary and discussion.

2 Non-Abelian chiral soliton lattices

In this section, we review the non-Abelian CSL in two-flavor QCD at finite baryon chemical potential μ_B and angular velocity $\boldsymbol{\Omega} = \Omega \hat{z}$ with flavor symmetric masses, $M = \text{diag}(m, m)$.

2.1 General setup

The chiral symmetry $U(2)_L \times U(2)_R$ of the two flavor QCD is

$$q_R \rightarrow e^{-i\tau_0 \theta_0^R} V_R q_R, \quad q_L \rightarrow e^{-i\tau_0 \theta_0^L} V_L q_L, \quad (2.1)$$

where $V_{R,L} \equiv \exp(-i\tau_A \theta_A^{R,L})$ are $SU(2)$ matrices with $U(2)$ generators τ_a with the normalization $\text{tr}(\tau_a \tau_b) = 2\delta_{ab}$. Here and below, the capital Latin letters run over 1, 2, 3, and the small letters run over 0, 1, 2, 3. We assume that this chiral symmetry is spontaneously broken down to the vector symmetry $U(2)_V$. Consequently, the η meson and pions appear as NG bosons which can be parametrized as

$$U = \Sigma \exp\left(\frac{i\tau_0 \eta}{f_\eta}\right), \quad \Sigma = \exp\left(\frac{i\tau_A \pi_A}{f_\pi}\right) \in SU(2), \quad (2.2)$$

with the decay constants $f_{\eta,\pi}$ of the η and π mesons. The field Σ transforms under $SU(2)_L \times SU(2)_R$ as

$$\Sigma \rightarrow V_L \Sigma V_R^\dagger, \quad (2.3)$$

while η transforms under $U(1)_A$ as

$$\eta \rightarrow \eta + 2f_\eta \theta_0 \quad (2.4)$$

where $\theta_0 \equiv \theta_0^R = -\theta_0^L$.

The effective Lagrangian for the η and π mesons is given by

$$\begin{aligned} \mathcal{L} = & \frac{1}{4} f_\pi^2 \text{tr}(\partial_\mu \Sigma \cdot \partial^\mu \Sigma^\dagger) + \frac{1}{2} (\partial_\mu \eta)^2 \\ & + \frac{Bm}{2} \text{tr}(U + U^\dagger - \mathbf{21}_2) + \frac{A}{2} (\det U + \det U^\dagger - \mathbf{21}_2) + \frac{\Omega \mu_B}{2\pi^2 N_c} \partial_z \left(\frac{\eta}{f_\eta} \right). \end{aligned} \quad (2.5)$$

More precisely, for the speeds of propagation of π and η in a medium are different in general, we should replace $\partial_\mu \partial^\mu \rightarrow \partial_t^2 - v_{\pi,\eta}^2 \nabla^2$ in the above Lagrangian. However, we will assume $v_\pi = v_\eta = 1$ in this paper for simplicity as in Ref. [9]. The first and second terms are the kinetic terms of the π and η mesons, respectively. They are invariant under $S[U(2)_L \times U(2)_R]$. The third term originates from explicit symmetry breaking due to the quark masses m . The pion mass m_π is related to the quark mass by $Bm = f_\pi^2 m_\pi^2/4$. It is invariant under the vector-like symmetry $SU(2)_V$ (taking $V_L = V_R$ in eq. (2.3)). The fourth term which is invariant under $SU(2)_L \times SU(2)_R$ corresponds to the $U(1)_A$ anomaly. The last term represents the anomalous coupling of the η meson to the rotation via the chiral anomaly. This term is derived by the anomaly matching for the CVE in terms of mesons [39, 40]. Hence, the Lagrangian symmetry is generally $SU(2)_V$.

The target space $U(2)$ is not simply connected. Since the first homotopy group is non-trivial as $\pi_1[U(2)] = \mathbb{Z}$, this system possesses topological solitons, non-Abelian sine-Gordon solitons [50, 51]. We will emphasize difference between $U(1) \times SU(2)$ and $U(2) \simeq \frac{U(1) \times SU(2)}{\mathbb{Z}_2}$.

For convenience, we will use the following quantities,

$$\sin\beta \equiv \frac{A}{C}, \quad \cos\beta \equiv \frac{2Bm}{C}, \quad C \equiv \sqrt{A^2 + (2Bm)^2}. \quad (2.6)$$

We assume both A and B are positive, so the range of β is $0 \leq \beta \leq \pi/2$. The potential term can be rewritten as

$$\mathcal{L}_{\text{pot}} \equiv -V_{\text{pot}} = C \left[\frac{1}{4} \cos\beta \cdot \text{tr}(U + U^\dagger - 2\mathbf{1}_2) + \sin\beta \cdot (\cos(2\eta/f_\eta) - 1) \right]. \quad (2.7)$$

In order to construct the ground state, we set $\pi_{1,2} = 0$ without the loss of generality due to the $SU(2)_V$ vector symmetry. Furthermore, we introduce dimensionless fields $\phi_{0,3}$ defined as $\phi_0 \equiv \eta/f_\eta$ and $\phi_3 \equiv \pi_3/f_\pi$, respectively, and the dimensionless variables,

$$\zeta \equiv \frac{\sqrt{C}z}{f_\eta}, \quad \epsilon \equiv 1 - \left(\frac{f_\pi}{f_\eta} \right)^2, \quad S \equiv \frac{\Omega\mu_B}{2\pi^2 N_c f_\eta \sqrt{C}}. \quad (2.8)$$

Then, eq. (2.7) reduces to

$$\frac{V_{\text{pot}}}{C} = \cos\beta(1 - \cos\phi_0 \cos\phi_3) + \sin\beta(1 - \cos 2\phi_0), \quad (2.9)$$

which is sketched in fig. 2. The potential is positive semi-definite because of the condition $0 \leq \beta \leq \pi/2$. Hence, the potential minimum is $V_{\text{pot}} = 0$. For $0 \leq \beta < \pi/2$ there are discrete minimum points at $(\phi_0, \phi_3) = (2n\pi, 2m\pi)$ and $((2n+1)\pi, (2m+1)\pi)$ with $n, m \in \mathbb{Z}$. Equivalently, these can also be represented as $(e^{i\phi_0}, \Sigma = e^{i\tau_A \phi_A}) = (1, \mathbf{1}_2)$ and $(-1, -\mathbf{1}_2)$. However, all these vacua are identical since they correspond to $U = \mathbf{1}_2$. The equivalence between $(1, \mathbf{1}_2)$ and $(-1, -\mathbf{1}_2)$ is nothing but the \mathbb{Z}_2 quotient of $U(2) \simeq \frac{U(1) \times SU(2)}{\mathbb{Z}_2}$. The potential flattens out in the direction of ϕ_3 as β increases from 0 to $\pi/2$, and it does not depend on ϕ_3 (explicitly speaking, V_{pot} is independent of Σ) at $\beta = \pi/2$. Therefore, the vacua at $\beta = \pi/2$ are the discrete straight lines at $\phi_0 = m\pi$ on the $\phi_0\phi_3$ plane.

As we will shortly explain below, this model admits topologically nontrivial states because the first homotopy group of the target space is nontrivial as $\pi_1[U(2)] \simeq \mathbb{Z}$. A

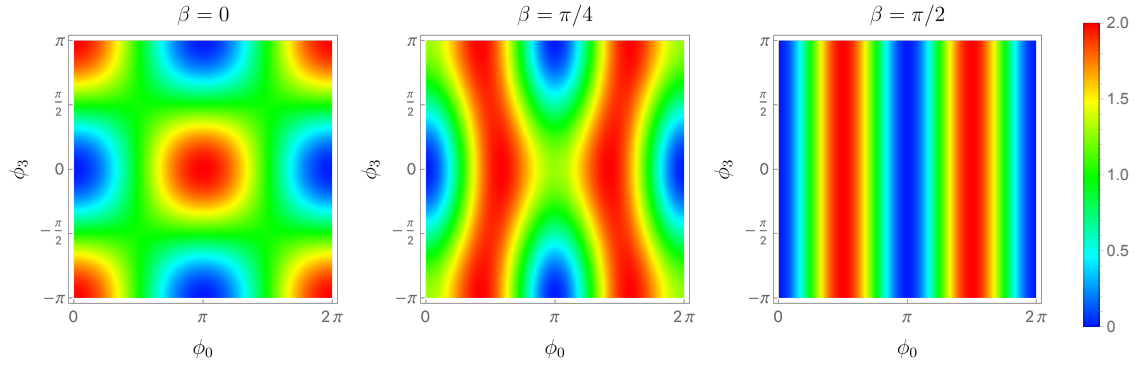


Figure 2. The density plot of the potential V_{pot}/C at $\beta = 0, \pi/4, \pi/2$, respectively. The horizontal lines of these graphs are ϕ_3 , and the vertical lines are ϕ_0 . As β increases, ϕ_3 -direction of V_{pot} flattens.

minimal loop is a U(1) orbit generated not by τ_0 but by the generator $\tau_+ = (\tau_0 + \tau_3)/2$. Namely, $U = e^{i\theta\tau_+} = \text{diag}(e^{i\theta}, 1)$ with $\theta \in [0, 2\pi]$. The loop corresponds to the red arrow connecting $(\phi_0, \phi_3) = (0, 0)$ and (π, π) in fig. 3 which is not homotopic to the trivial loop $U = \mathbf{1}_2$. $U = e^{i\tau_0\theta}$ is also a nontrivial loop corresponding to the black arrow between $(0, 0)$ and $(2\pi, 0)$ in fig. 3 but this is not minimal because it winds twice about the target space $U(2)$. It is important to realize that the minimal loop is infinitely degenerate because $U' = V e^{i\tau_+\theta} V^\dagger$ with an arbitrary $V \in \text{SU}(2)$ obviously has the same property as $U = e^{i\tau_+\theta}$. For example, if we take $V = i\tau_1$, we have $U' = e^{i\tau_-\theta}$ with $\tau_- = (\tau_0 - \tau_3)/2$ which corresponds to the blue arrow between $(0, 0)$ and $(\pi, -\pi)$ in fig. 3.

Accordingly, kinks exist corresponding to the nontrivial loops. Let us call the kinks with $e^{i\theta\tau_+}$ and $e^{i\theta\tau_-}$ an up and down soliton, respectively. They are continuously connected by an $\text{SU}(2)_V$ transformation as explained above. An important property of this soliton is that it has not only a translational moduli but also the S^2 moduli. To illustrate this, let us consider an up soliton $U = e^{i\tau_+\theta}$. The vacua ($U = \mathbf{1}_2$) are $\theta = 0$ and 2π , and the kink center has $\theta = \pi$ ($U = -\tau_3$). Therefore, the $\text{SU}(2)$ symmetry is spontaneously broken up to the U(1) one only around the up soliton. Therefore, this soliton has the localized moduli of $\text{SU}(2)/\text{U}(1) \simeq S^2$. In this way, the kink has internal degrees of freedom and is different from the usual sine-Gordon kink.

The kink itself naturally has a spatial dependence and usually has more energy than the vacuum state. However, in this case, the fifth term of eq. (2.5) reduces the energy of the modulating coordination in the z direction. In the following, we consider only the dependence in the z direction in order to investigate the possibility that a soliton appears in the ground state. Hence, the reduced Hamiltonian density is calculated as

$$\frac{\mathcal{H}}{C} = \frac{1-\epsilon}{2}(\phi_3')^2 + \frac{1}{2}(\phi_0')^2 + \sin\beta(1 - \cos 2\phi_0) + \cos\beta(1 - \cos\phi_0 \cos\phi_3) - S\phi_0', \quad (2.10)$$

where the prime denotes the differentiation with respect to ζ .

It is useful to change the basis by

$$\phi_{\pm} \equiv \phi_0 \pm \phi_3. \quad (2.11)$$

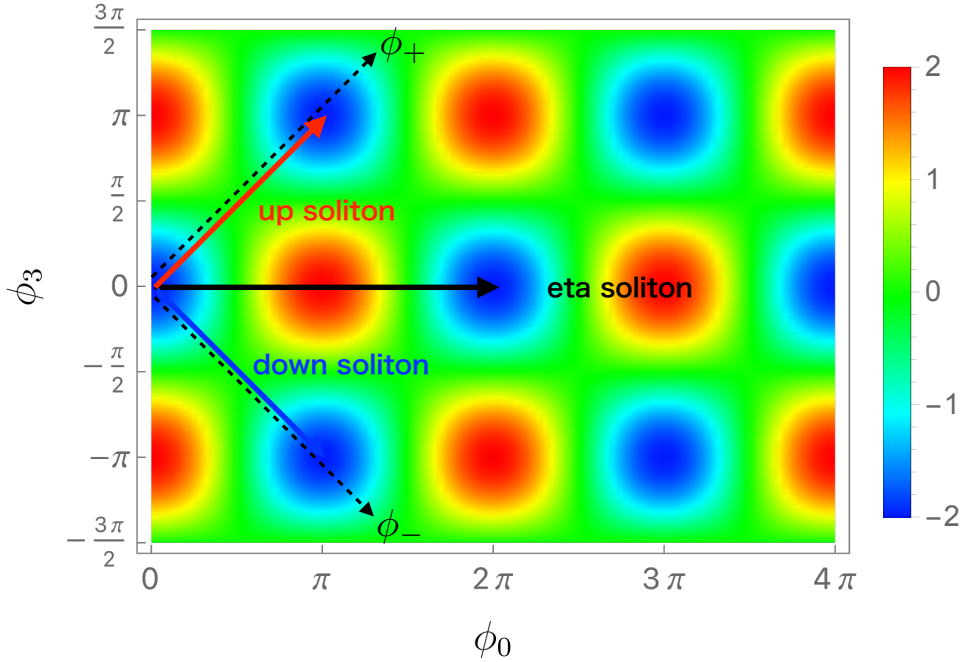


Figure 3. Schematic picture of an arrangement of the up (red arrow) and down (blue arrow) solitons. Since $\ell_+ = \ell_- = \ell$, the state where the up and down solitons farthest apart satisfies $d = \ell/2$. This state is called the deconfined phase. On the other hand, the state where the up and down solitons are completely overlapped (the black arrow) is called the confined phase. The intermediate state satisfies $d < \ell/2$.

Using these bases, the Hamiltonian can be written as

$$\begin{aligned} \frac{\mathcal{H}}{C} = & \frac{1}{2} \left[\frac{1 - \epsilon/2}{2} (\phi'_+)^2 + \cos \beta (1 - \cos \phi_+) - S\phi'_+ \right] \\ & + \frac{1}{2} \left[\frac{1 - \epsilon/2}{2} (\phi'_-)^2 + \cos \beta (1 - \cos \phi_-) - S\phi'_- \right] \\ & + \frac{\epsilon}{4} \phi'_+ \phi'_- + \sin \beta (1 - \cos(\phi_+ + \phi_-)), \end{aligned} \quad (2.12)$$

where we have used the following equation

$$-\frac{\epsilon}{2} (\phi'_3)^2 = -\frac{\epsilon}{8} (\phi'_+)^2 - \frac{\epsilon}{8} (\phi'_-)^2 + \frac{\epsilon}{4} \phi'_+ \phi'_-. \quad (2.13)$$

2.2 The noninteractive case of $\epsilon = 0$ and $\beta = 0$

In this subsection, we consider the simplest case of $\epsilon = 0$ and $\beta = 0$. The Hamiltonian in eq. (2.12) is reduced in this case to

$$\frac{\mathcal{H}}{C} = \frac{1}{2} \left[\frac{(\phi'_+)^2}{2} + (1 - \cos \phi_+) - S\phi'_+ \right] + \frac{1}{2} \left[\frac{(\phi'_-)^2}{2} + (1 - \cos \phi_-) - S\phi'_- \right]. \quad (2.14)$$

Therefore, ϕ_{\pm} are completely decoupled, and each Hamiltonian is a half of that of ϕ_0 (see eq. (2.10) at $\epsilon = 0$ and $\beta = 0$). The equation of motion of ϕ_{\pm} is

$$\phi''_{\pm} = \sin \phi_{\pm}, \quad (2.15)$$

which can be analytically solved by using the Jacobi's elliptic function as

$$\phi_{\pm} = 2\text{am}\left(\frac{\zeta - \zeta_{\pm}}{k_{\pm}}\right) + \pi, \quad (2.16)$$

where k_{\pm} ($0 < k_{\pm} < 1$) is the elliptic modulus, and ζ_{\pm} are translational moduli of the up and down CSLs. The period of each solution is given by

$$\ell_{\pm} = 2k_{\pm}K(k_{\pm}), \quad (2.17)$$

where $K(k)$ is the complete elliptic integral of the first kind. The elliptic moduli k_{\pm} are determined by an energy minimization condition as follows. Substituting eq. (2.16) into the Hamiltonian in eq. (2.14), we can calculate the CSL energy for one period which depends on k_{\pm} . The minimization condition of this energy turns out to be

$$\frac{E(k_{\pm})}{k_{\pm}} = \frac{\pi S}{4}, \quad (2.18)$$

where $E(k_{\pm})$ is the complete elliptic integral of the second kind. This determines k_{\pm} for a given angular velocity S . Combining this and eq. (2.17), one can get ℓ_{\pm} as a function of S with k_{\pm} being the parameters. Since the elliptic integral satisfies the inequality $E(k_{\pm})/k_{\pm} \geq 1$, we are led to the condition $S \geq 4/\pi$. Hence the critical angular velocity S_c is given by

$$S_c = \frac{4}{\pi}. \quad (2.19)$$

Since the right-hand side of eq. (2.18) of the up and down solitons are respectively equal, we show $k_+ = k_-$ and $\ell_+ = \ell_- \equiv \ell$. We emphasize that the CSL state is energetically more stable than the vacuum state $\phi_{\pm} = 0$ when $S \geq S_c$ is satisfied.

The relative distance d is a free parameter for $\epsilon = \beta = 0$. On the other hand, when we turn on ϵ and β , d is no longer free to be chosen since the up and down solitons interact with each other. The distance d is dynamically determined. The states with $d = \ell/2$, $d < \ell/2$, and $d = 0$ are called a deconfined, dimer, and confined phases, respectively (see fig. 1).

2.3 Confined phase

In this section, we first explain the effects of the term depending on $\epsilon > 0$. Since the kink solution of ϕ_{\pm} has the leak at the center of the kink, the interaction between up and down kinks is repulsive due to the third term in eq. (2.13). The ϵ -dependence of ϕ_{\pm} is described in the left panel of fig. 4. As ϵ increases, the distance between ϕ_+ and ϕ_- also increases.

We next explain the effects of the third and fourth terms in eq. (2.10). This potential is sketched in fig. 2. As β increases, the ϕ_3 direction becomes flat. Therefore, modulation in ϕ_3 is suppressed at small ϵ (large β) (see the left panel of fig. 4).

Therefore, a non-zero positive ϵ yields a repulsive force between the up and down solitons, whereas a non-zero positive β leads to an attractive inter-soliton force. When β is sufficiently larger than ϵ such that the attraction dominates over the repulsion, the up and down solitons overlap entirely, then $d = 0$. This phase corresponds to the confined phase (see the third line of fig. 1). This soliton is nothing but an η soliton (ϕ_3 is identically zero) not spontaneously breaking the isospin symmetry $SU(2)_V$ and thus is called an Abelian soliton.

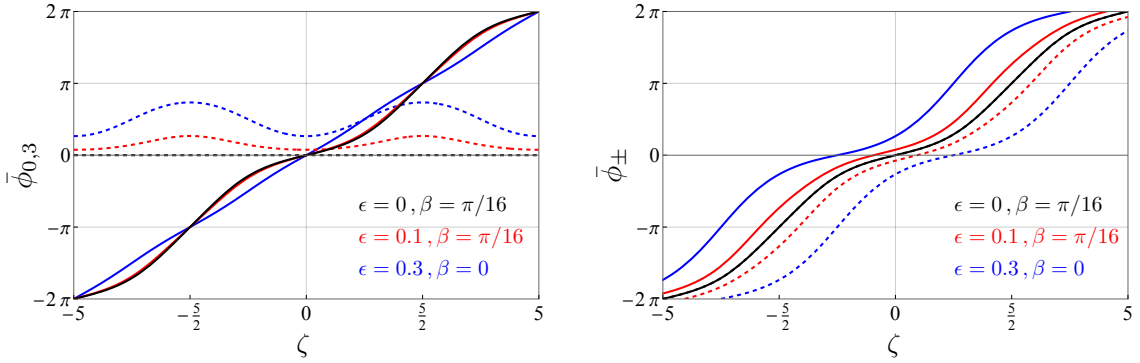


Figure 4. Numerical solution of $\chi_{0,3}$ (left panel) and χ_{\pm} (right panel) for $\ell = 5$. The black, red, and blue lines correspond to the confined, dimer, and deconfined phases, respectively. The solid (dashed) curves show $\chi_0(\chi_3)$ in the left panel, and $\chi_+(\chi_-)$ in the right one.

2.4 Deconfined phase

We next consider the case where the repulsive force is sufficiently large that the up and down solitons separate as far apart as possible. In this situation, the up and down solitons alternatively align with equal distance $d = \ell/2$ as sketched in the first line of fig. 1. One of the important differences between the confined and deconfined phases is that not only ϕ_0 but also ϕ_3 have the nontrivial kink profiles in the latter case. Therefore, the non-Abelian part (or $\Sigma \in \text{SU}(2)$) has a nontrivial expectation value, and then this state is called the non-Abelian CSL. The other is that the isospin symmetry $\text{SU}(2)_V$ is spontaneously broken down to $\text{U}(1)$. Hence, the NG modes associated with this spontaneous symmetry breaking appear in the vicinity of the soliton. Consequently, each soliton has the moduli $S^2 \simeq \text{SU}(2)_V/\text{U}(1)$. We also note that the deconfined phase has a discrete symmetry under the d shift in the z direction, replacing the up (down) soliton with the down (up) one, as expressed by

$$z \rightarrow z - d, \quad \tau_1 \text{diag}(\phi_+, \phi_-) \tau_1 = \text{diag}(\phi_-, \phi_+). \quad (2.20)$$

2.5 Dimer phase

Finally, let us consider the case where attractive and repulsive forces are balanced. In this situation, the up and down solutions are neither completely separate nor completely overlapping. The up and down solitons form a molecule whose size d satisfies $0 < d < \ell/2$. Then, we call this state the dimer phase. The isospin symmetry $\text{SU}(2)_V$ is spontaneously broken down to $\text{U}(1)$ as in the deconfined phase. Therefore, it is noteworthy that the isospin also appears as the NG bosons. On the other hand, the dimer phase does not have the discrete symmetry (2.20) because of $\ell/2 \neq d$.

3 Dispersion relations around chiral soliton lattices

The CSL is the one-dimensional crystal of the kinks. Similar to an ordinary crystal of atoms, quasi particles like phonons propagate through the CSL. The Abelian CSL of the η meson is essentially identical to the well-known soliton lattice in the sine-Gordon model,

and the dispersion relation of excitation modes was clarified in Ref. [66]. In contrast, the non-Abelian CSL includes a rich spectrum. In this section, we study fluctuations around the CSL phases to numerically obtain dispersion relations for NG modes and gapful modes. After deriving equations for fluctuations in the background of the CSLs, we study the noninteractive case of $\epsilon = 0$ and $\beta = 0$, confined phase (η -CSL), deconfined phase and dimer phase in each subsection.

3.1 Equations of motion for fluctuations

In order to calculate the dispersion relations of the NG modes in the non-Abelian CSLs, we approximate eq. (2.5) up to the quadratic of fluctuations from the background configurations $\{\bar{\phi}_0, \bar{\phi}_3\}$ with the following boundary condition:

$$\bar{\phi}_0(0) = 0, \quad \bar{\phi}_0(\ell) = 2\pi, \quad (3.1)$$

$$\bar{\phi}'_3(0) = \bar{\phi}'_3(\ell) = 0, \quad (3.2)$$

where ℓ is a period of the kinks, see fig. 4 (a). We introduce small fluctuations as follows:

$$\Sigma = e^{i\tau_3 \bar{\phi}_3} \delta\Sigma, \quad \eta/f_\eta = \phi_0 = \bar{\phi}_0 + \delta\phi_0 \quad (3.3)$$

where the fluctuation of the SU(2) part satisfies $\det \delta\Sigma = 1$ due to the condition $\det \Sigma = 1$. Then, we can represent $\delta\Sigma$ as

$$\delta\Sigma = \sqrt{1 - \delta\phi_A^2} + i\tau_A \delta\phi_A. \quad (3.4)$$

$\delta\Sigma\delta\Sigma^\dagger = \mathbf{1}_2$ is also satisfied. Substituting the above equations into eq. (2.5), the Lagrangian of the quadratic order in the fluctuations is given by

$$\begin{aligned} \mathcal{L}^{(2)} = & \frac{f_\eta^2}{2} (\partial_\mu \delta\phi_0)^2 + \frac{f_\pi^2}{2} (\partial_\mu \delta\phi_A)^2 - f_\pi^2 \epsilon_{3AB} \partial_\mu \bar{\phi}_3 \delta\phi_A \partial^\mu \delta\phi_B \\ & + \frac{C \cos \beta}{2} (-\delta\phi_a^2 \cos \bar{\phi}_0 \cos \bar{\phi}_3 + 2\delta\phi_0 \delta\phi_3 \sin \bar{\phi}_0 \sin \bar{\phi}_3) \\ & - 2C \sin \beta \cos 2\bar{\phi}_0 \delta\phi_0^2, \end{aligned} \quad (3.5)$$

This can be separated into two decoupled portions as

$$\begin{aligned} \mathcal{L}_{\text{neutral}}^{(2)} = & \frac{f_\eta^2}{2} (\partial_\mu \delta\phi_0)^2 + \frac{f_\pi^2}{2} (\partial_\mu \delta\phi_3)^2 - 2C \sin \beta \cos 2\bar{\phi}_0 \delta\phi_0^2 \\ & + \frac{C \cos \beta}{2} [-(\delta\phi_0^2 + \delta\phi_3^2) \cos \bar{\phi}_0 \cos \bar{\phi}_3 + 2\delta\phi_0 \delta\phi_3 \sin \bar{\phi}_0 \sin \bar{\phi}_3], \end{aligned} \quad (3.6)$$

$$\begin{aligned} \mathcal{L}_{\text{charged}}^{(2)} = & \frac{f_\pi^2}{2} [(\partial_\mu \delta\phi_1)^2 + (\partial_\mu \delta\phi_2)^2] - f_\pi^2 \epsilon_{3AB} \partial_\mu \bar{\phi}_3 \delta\phi_A \partial^\mu \delta\phi_B \\ & - \frac{C \cos \beta}{2} \cos \bar{\phi}_0 \cos \bar{\phi}_3 (\delta\phi_1^2 + \delta\phi_2^2), \end{aligned} \quad (3.7)$$

We refer the neutral components $\delta\phi_{0,3}$ to phonons because they are related to the NG and quasi-NG bosons associated with the spontaneously broken translational symmetry by the CSL. On the other hand, we call the charged fluctuations $\delta\phi_{1,2}$ as the isospinons [42] are the NG bosons because they are associated with the spontaneously broken isospin symmetry $SU(2)_V$ by the background $\bar{\phi}_3 \neq 0$.

3.1.1 The neutral components: phonons

The linearized EOM of $\delta\phi_0$ is given by

$$(\partial_{\bar{t}}^2 - \partial_{\zeta}^2) \delta\phi_0 + (4 \sin \beta \cos 2\bar{\phi}_0 + \cos \beta \cos \bar{\phi}_0 \cos \bar{\phi}_3) \delta\phi_0 - (\cos \beta \sin \bar{\phi}_0 \sin \bar{\phi}_3) \delta\phi_3 = 0, \quad (3.8)$$

where we have used dimensionless variables in eq. (2.8), the dimensionless coordinate defined as $\bar{t} \equiv \sqrt{C}t/f_\eta$. Similarly, the linearized EOM for $\delta\phi_3$ reads

$$(1 - \epsilon) (\partial_{\bar{t}}^2 - \partial_{\zeta}^2) \delta\phi_3 - (\cos \beta \sin \bar{\phi}_0 \sin \bar{\phi}_3) \delta\phi_0 + (\cos \beta \cos \bar{\phi}_0 \cos \bar{\phi}_3) \delta\phi_3 = 0. \quad (3.9)$$

Note that we have assumed the fluctuations depend only on t and z for simplicity.³

We first focus on the neutral components ϕ_0 and ϕ_3 . It turns out that the following redefinition of the fields is useful

$$\delta\phi_+ \equiv \delta\phi_0 + \delta\phi_3, \quad \delta\phi_- \equiv \delta\phi_0 - \delta\phi_3. \quad (3.10)$$

In terms of these new fields, together with the decomposition

$$\delta\phi_{\pm} = e^{-i\bar{\omega}\bar{t}} \varphi_{\pm}(\zeta), \quad (3.11)$$

the linearized EOMs reduce

$$\left[-\partial_{\zeta}^2 + \begin{pmatrix} P_+ & Q_- \\ Q_+ & P_- \end{pmatrix} \right] \begin{pmatrix} \varphi_+ \\ \varphi_- \end{pmatrix} = \bar{\omega}^2 \begin{pmatrix} \varphi_+ \\ \varphi_- \end{pmatrix}, \quad (3.12)$$

with

$$P_{\pm} = 2 \sin \beta \cos 2\bar{\phi}_0 + \frac{2 - \epsilon}{2(1 - \epsilon)} \cos \beta \cos \bar{\phi}_{\pm}, \quad (3.13)$$

$$Q_{\pm} = 2 \sin \beta \cos 2\bar{\phi}_0 - \frac{\epsilon}{2(1 - \epsilon)} \cos \beta \cos \bar{\phi}_{\pm}. \quad (3.14)$$

In order to find a collect dispersion relation, we should take the periodicity of the potential into account. The common periodicity in ζ among $\cos 2\bar{\phi}_0$ and $\cos \bar{\phi}_3$ is the lattice constant ℓ , so that P_{\pm} and Q_{\pm} have the same periodicity. Hence, this equation has a form similar to the Schrödinger equation for electrons in a crystal. Therefore, we can apply the Bloch theorem to our system, and $\varphi_{\pm}(\zeta)$ satisfies the following equation:

$$\varphi_{\pm}(\zeta + \ell) = e^{i\bar{p}\ell} \varphi_{\pm}(\zeta), \quad (3.15)$$

where \bar{p} is a dimensionless crystal momentum vector. We consider the periodic boundary condition, which is the so-called Born–von Karman boundary condition:

$$\varphi_{\pm}(\zeta + N\ell) = \varphi_{\pm}(\zeta) \quad (3.16)$$

³Including x^1 and x^2 makes the fluctuation analysis much more complicated due to the rotation effect in the metric.

where N is a positive integer. Substituting eq. (3.16) into eq. (3.15), we get $e^{i\bar{p}N\ell} = 1$. As a result, the crystal momentum \bar{p} takes discrete values as

$$\bar{p}_n = \frac{2\pi n}{N\ell} \quad (n \in \mathbb{Z}). \quad (3.17)$$

In fact, it is sufficient to consider \bar{p}_n in the following range

$$-\frac{\pi}{\ell} < \bar{p}_n \leq \frac{\pi}{\ell}. \quad (3.18)$$

This is called the first Brillouin zone which is a unit cell of the reciprocal lattice. Note that, when we replace p_n with $\bar{p}_n + 2\pi j/\ell$ ($j \in \mathbb{Z}$), $\varphi_{\pm}(\zeta)$ satisfies the following equation due to the Bloch theorem:

$$\varphi_{\pm}(\zeta + \ell) = e^{i(\bar{p}_n + g_j)\ell} \varphi_{\pm}(\zeta) = e^{i\bar{p}_n\ell} \varphi_{\pm}(\zeta), \quad (3.19)$$

where we define $g_j \equiv 2\pi j/\ell$ corresponding to the reciprocal lattice vector. Hence, this momentum shift simply leads back to the same wave function. This implies that there are multiple $\varphi_{\pm}(\zeta)$ for the same \bar{p}_n in the first Brillouin zone. We will use the label j to distinguish them (j is a label specifying the band structure). For later convenience, we define $u_{\pm}^{(n)}(\zeta)$ as follow

$$\varphi_{\pm}^{(n)}(\zeta) = e^{i\bar{p}_n\zeta} u_{\pm}^{(n)}(\zeta), \quad (3.20)$$

where we impose $u_{\pm}^{(n)}(\zeta + \ell) = u_{\pm}^{(n)}(\zeta)$. Inserting eq. (3.20) into eq. (3.12), we get the Schrödinger equation for $u_{\pm}^{(n)}$

$$\left[-(\partial_{\zeta} + i\bar{p}_n)^2 + \begin{pmatrix} P_+ & Q_- \\ Q_+ & P_- \end{pmatrix} \right] \begin{pmatrix} u_+^{(n)} \\ u_-^{(n)} \end{pmatrix} = \bar{\omega}_{(n,j)}^2 \begin{pmatrix} u_+^{(n)} \\ u_-^{(n)} \end{pmatrix}. \quad (3.21)$$

Below, we will attempt to numerically solve eq. (3.21). To this end, it is convenient to perform the Fourier expansion of eq. (3.21). Since $u_{\pm}^{(n)}$ has a period ℓ , it can be expanded by the Fourier series as

$$u_{\pm}^{(n)}(\zeta) = \sum_m f_{\pm}^{(n;m)} e^{i\frac{2\pi m}{\ell}\zeta} = \sum_m f_{\pm}^{(n;m)} e^{igm\zeta}. \quad (3.22)$$

Then, the derivative term is expanded as

$$-(\partial_{\zeta} + i\bar{p}_n)^2 u_{\pm}^{(n)}(\zeta) = \sum_m (\bar{p}_n + g_m)^2 f_{\pm}^{(n;m)} e^{igm\zeta}. \quad (3.23)$$

Similarly, we expand the background functions $\bar{\phi}_0$ and $\bar{\phi}_{\pm}$ and express them as

$$\cos \bar{\phi}_{\pm} = \sum_n c_{\pm}^{(n)} e^{i\frac{2\pi n}{\ell}\zeta} = \sum_n c_{\pm}^{(n)} e^{ign\zeta}, \quad (3.24)$$

$$\cos 2\bar{\phi}_0 = \sum_n c_0^{(n)} e^{i\frac{2\pi n}{\ell}\zeta} = \sum_n c_0^{(n)} e^{ign\zeta}. \quad (3.25)$$

So, for example, the Fourier expansion of $u_{\pm}^{(n)} \cos \bar{\phi}_{\pm}$ is given by

$$u_{\pm}^{(n)} \cos \bar{\phi}_{\pm} = \sum_{m,m'} f_{\pm}^{(n;m)} c_{\pm}^{(m')} e^{i(g_m + g_{m'})\zeta} = \sum_m \left(\sum_{m'} c_{\pm}^{(m')} f_{\pm}^{(n;m-m')} \right) e^{ig_m \zeta}. \quad (3.26)$$

Similar expressions can be easily obtained for the other terms $u_{\pm}^{(n)} \cos 2\bar{\phi}_0$. Then, we get the Fourier series of the left-hand side of eq. (3.12)

$$- \frac{d^2}{d\zeta^2} u_+^{(n)} + P_+ u_+^{(n)} + Q_- u_-^{(n)} = \sum_m e^{ig_n \zeta} \left\{ (\bar{p}_n + g_m)^2 f_+^{(n;m)} + \sum_{m'} \left(A_+^{(m')} f_+^{(n;m-m')} + B_-^{(m')} f_-^{(n;m-m')} \right) \right\}, \quad (3.27)$$

$$- \frac{d^2}{d\zeta^2} u_-^{(n)} + Q_+ u_+^{(n)} + P_- u_-^{(n)} = \sum_m e^{ig_n \zeta} \left\{ (\bar{p}_n + g_m)^2 f_-^{(n;m)} + \sum_{m'} \left(B_+^{(m')} f_+^{(n;m-m')} + A_-^{(m')} f_-^{(n;m-m')} \right) \right\}. \quad (3.28)$$

with

$$A_{\pm}^{(m)} \equiv 2c_0^{(m)} \sin \beta + \frac{2 - \epsilon}{2(1 - \epsilon)} c_{\pm}^{(m)} \cos \beta, \quad (3.29)$$

$$B_{\pm}^{(m)} \equiv 2c_0^{(m)} \sin \beta - \frac{\epsilon}{2(1 - \epsilon)} c_{\pm}^{(m)} \cos \beta. \quad (3.30)$$

Plugging all these into eq. (3.12), we eventually find

$$\bar{\omega}_{(n)}^2 f_+^{(n;m)} = (\bar{p}_n + g_m)^2 f_+^{(n;m)} + \sum_{m'} \left(A_+^{(m')} f_+^{(n;m-m')} + B_-^{(m')} f_-^{(n;m-m')} \right), \quad (3.31)$$

$$\bar{\omega}_{(n)}^2 f_-^{(n;m)} = (\bar{p}_n + g_m)^2 f_-^{(n;m)} + \sum_{m'} \left(B_+^{(m')} f_+^{(n;m-m')} + A_-^{(m')} f_-^{(n;m-m')} \right). \quad (3.32)$$

One can see that $f_{\pm}^{(n;m)}$ couples only to $f_{\pm}^{(n';m')}$ with $n' = n$. Composing $f_{\pm}^{(n;m)}$ into the following vectors

$$\mathbf{f}_{\pm}^{(n)} \equiv \left(\dots, f_{\pm}^{(n;2)}, f_{\pm}^{(n;1)}, f_{\pm}^{(n;0)}, f_{\pm}^{(n;-1)}, f_{\pm}^{(n;-2)}, \dots \right)^T, \quad (3.33)$$

eqs. (3.31) and (3.32) are cast into the matrix equation

$$\bar{\omega}_{(n)}^2 \begin{pmatrix} \mathbf{f}_+^{(n)} \\ \mathbf{f}_-^{(n)} \end{pmatrix} = \begin{pmatrix} C_+^{(n)} & D_- \\ D_+ & C_-^{(n)} \end{pmatrix} \begin{pmatrix} \mathbf{f}_+^{(n)} \\ \mathbf{f}_-^{(n)} \end{pmatrix}, \quad (3.34)$$

with

$$C_{\pm}^{(n)} \equiv \begin{pmatrix} \ddots & & & & \\ & (\bar{p}_n + g_{-1})^2 & & & \\ & & \bar{p}_n^2 & & \\ & & & (\bar{p}_n + g_1)^2 & \\ & & & & \ddots \end{pmatrix} + \begin{pmatrix} \vdots & \vdots & \vdots & & \\ \cdots & A_{\pm}^{(0)} & A_{\pm}^{(-1)} & A_{\pm}^{(-2)} & \cdots \\ \cdots & A_{\pm}^{(1)} & A_{\pm}^{(0)} & A_{\pm}^{(-1)} & \cdots \\ \cdots & A_{\pm}^{(2)} & A_{\pm}^{(1)} & A_{\pm}^{(0)} & \cdots \\ \vdots & \vdots & \vdots & & \end{pmatrix}, \quad (3.35)$$

$$D_{\pm} \equiv \begin{pmatrix} \vdots & \vdots & \vdots & & \\ \cdots & B_{\pm}^{(0)} & B_{\pm}^{(-1)} & B_{\pm}^{(-2)} & \cdots \\ \cdots & B_{\pm}^{(1)} & B_{\pm}^{(0)} & B_{\pm}^{(-1)} & \cdots \\ \cdots & B_{\pm}^{(2)} & B_{\pm}^{(1)} & B_{\pm}^{(0)} & \cdots \\ \vdots & \vdots & \vdots & & \end{pmatrix}. \quad (3.36)$$

The prescription for finding the dispersion relation is the following. We first choose n in $-N/2 < n \leq N/2$ or the corresponding momentum \bar{p}_n in the Brillouin zone. Then we solve the eigen-equation (3.34), and determine the eigenvalues $\bar{\omega}_{(n,j)}$ and eigenvector $\mathbf{f}_{\pm}^{(n,j)}$. We repeat this for each n in $-N/2 < n \leq N/2$. Note that for the chosen momentum \bar{p}_n , there are multiple states labeled by the new index j . The label j is nothing but the index associated with the band structure. Though the sizes of matrices $C_{\pm}^{(n)}$ and D_{\pm} are infinite, we have to truncate them to be finite-size matrices for numerical computations. We denote the finite-size matrices as

$$\left(\tilde{C}_{\pm}^{(n)}\right)_{ij} = (\bar{p}_n + g_{i-d-1})\delta_{ij} + A_{\pm}^{(i-j)}, \quad (3.37)$$

$$\left(\tilde{D}_{\pm}^{(n)}\right)_{ij} = B_{\pm}^{(i-j)}, \quad (3.38)$$

where i, j are indices of the truncated matrices running over $1, 2, \dots, 2\Lambda + 1$. Upon diagonalizing the matrix, we derive $2(2\Lambda + 1)$ eigenvalues. These are distinguished by the label j , which denotes the band index. For convenience in subsequent discussions, we arrange j in the order $j = 1, 2, \dots, 2(2\Lambda + 1)$ such that

$$|\bar{\omega}_{(n,j=1)}| \leq |\bar{\omega}_{(n,j=2)}| \leq |\bar{\omega}_{(n,j=3)}| \cdots \leq |\bar{\omega}_{(n,j=2(2\Lambda+1))}|. \quad (3.39)$$

3.1.2 The charged components: isospinons

The linearized EOM of $\delta\phi_1$ and $\delta\phi_2$ are given by

$$f_{\pi}^2 (\partial_{\mu}^2 \delta\phi_1 + \partial_{\mu}^2 \bar{\phi}_3 \delta\phi_2 + 2\partial_{\mu} \bar{\phi}_3 \partial^{\mu} \delta\phi_2) + C \cos \beta \cos \bar{\phi} \cos \bar{\phi}_3 \delta\phi_1 = 0, \quad (3.40)$$

$$f_{\pi}^2 (\partial_{\mu}^2 \delta\phi_2 - \partial_{\mu}^2 \bar{\phi}_3 \delta\phi_1 - 2\partial_{\mu} \bar{\phi}_3 \partial^{\mu} \delta\phi_1) + C \cos \beta \cos \bar{\phi} \cos \bar{\phi}_3 \delta\phi_2 = 0. \quad (3.41)$$

These can be combined into a complex equation for $\delta\pi_{\pm} \equiv \delta\phi_1 \pm i\delta\phi_2$ as

$$f_{\pi}^2 (\partial_{\mu}^2 \delta\pi_{+} - i(\partial_{\mu}^2 \bar{\phi}_3) \delta\pi_{+} - 2i(\partial_{\mu} \bar{\phi}_3) \partial^{\mu} \delta\pi_{+}) + C \cos \beta \cos \bar{\phi} \cos \bar{\phi}_3 \delta\pi_{+} = 0. \quad (3.42)$$

This can be further simplified by introducing the following field:

$$\delta\tilde{\pi}_+ \equiv e^{-i\bar{\phi}_3} \delta\pi_+. \quad (3.43)$$

Eq. (3.42) is rewritten as

$$\partial_\mu^2 \delta\tilde{\pi}_+ - (\partial_z \bar{\phi}_3)^2 \delta\tilde{\pi}_+ + \frac{C}{f_\pi^2} \cos \beta \cos \bar{\phi}_0 \cos \bar{\phi}_3 \delta\tilde{\pi}_+ = 0. \quad (3.44)$$

Using the dimensionless variables and decomposing the fluctuation as

$$\delta\tilde{\pi}_+ = e^{-i\bar{\ell}\bar{\omega}} \psi_+(\zeta), \quad (3.45)$$

we finally obtain

$$\left\{ -\partial_\zeta^2 - (\partial_\zeta \bar{\phi}_3)^2 + \frac{\cos \beta}{1-\epsilon} \cos \bar{\phi}_0 \cos \bar{\phi}_3 \right\} \psi_+ = \bar{\omega}^2 \psi_+. \quad (3.46)$$

The potential is periodic with the periodicity ℓ as before. So ψ_+ satisfies the Bloch theorem

$$\psi_+(\zeta + \ell) = e^{i\bar{p}\zeta} \psi_+(\zeta), \quad (3.47)$$

where \bar{p} is a real number. We impose the Born-Von Karman boundary condition

$$\psi_+(\zeta + N\ell) = \psi_+(\zeta), \quad (3.48)$$

with an integer N . Then, \bar{p} is quantized as eq. (3.17). Just as in the case of φ_\pm , it is enough for us to take the momentum \bar{p}_n in the first Brillouin zone (3.18). Hereafter, we will denote the wave function $\psi_+^{(n)}$ with the index n to specify the crystal momentum \bar{p}_n . But, as mentioned above, there are multiple $\psi_+^{(n)}$ for the same \bar{p}_n due to the symmetry (3.19), which will be distinguished by the band index j . In order to obtain the dispersion relation numerically, let us rewrite $\psi_+^{(n)}$ as

$$\psi_+^{(n)}(\zeta) = e^{i\bar{p}_n \zeta} v_+^{(n)}(\zeta), \quad (3.49)$$

where $v_+^{(n)}(\zeta + \ell) = v_+^{(n)}(\zeta)$ is imposed. Substituting this equation in eq. (3.46), we get the EOM for $v_+^{(n)}$ given by

$$[-(\partial_\zeta + ip_n)^2 + R(\zeta)] v_+^{(n)} = \bar{\omega}_{(n)}^2 v_+^{(n)}, \quad (3.50)$$

with

$$R(\zeta) \equiv -(\partial_\zeta \bar{\phi}_3)^2 + \frac{\cos \beta}{1-\epsilon} \cos \bar{\phi}_0 \cos \bar{\phi}_3. \quad (3.51)$$

Since $R(\zeta)$ has a period ℓ , it is expanded as

$$R(\zeta) = \sum_m r_m e^{igm\zeta}. \quad (3.52)$$

Denoting the Fourier expansion of $v_+^{(n)}$ as

$$v_{\pm}^{(n)}(\zeta) = \sum_m g_{\pm}^{(n;m)} e^{i2\pi m\zeta/\ell} = \sum_m g_{\pm}^{(n;m)} e^{igm\zeta}, \quad (3.53)$$

$v_+^{(n)}R$ can be calculated as

$$v_{\pm}^{(n)}R = \sum_m \left(\sum_{m'} r_{\pm}^{(m')} g_{\pm}^{(n;m-m')} \right) e^{igm\zeta} \quad (3.54)$$

Then, we get the Fourier series of eq. (3.50)

$$\bar{\omega}_{(n)}^2 g_+^{(n;m)} = (\bar{p}_n + g_m)^2 g_+^{(n;m)} + \sum_{m'} r^{(m')} g_+^{(n;m-m')}. \quad (3.55)$$

It is evident that $g_+^{(n;m)}$ couples only with $g_+^{(n';m')}$ with $n = n'$. By expressing $g_+^{(n;m)}$ as the vector

$$\mathbf{g}_+^{(n)} \equiv \left(\dots, g_+^{(n;2)}, g_+^{(n;1)}, g_+^{(n;0)}, g_+^{(n;-1)}, g_+^{(n;-2)}, \dots \right)^T, \quad (3.56)$$

eq. (3.55) can be reformulated as a matrix equation as follows:

$$\bar{\omega}_{(n)}^2 \mathbf{g}_+^{(n)} = E^{(n)} \mathbf{g}_+^{(n)}, \quad (3.57)$$

where the matrix $E^{(n)}$ is defined as

$$E^{(n)} \equiv \begin{pmatrix} \ddots & & & & & & \\ & (\bar{p}_n + g_{-1})^2 & & & & & \\ & & \bar{p}_n^2 & & & & \\ & & & (\bar{p}_n + g_1)^2 & & & \\ & & & & \ddots & & \\ & & & & & & \end{pmatrix} + \begin{pmatrix} & \vdots & \vdots & \vdots & & & \\ \dots & r^{(0)} & r^{(-1)} & r^{(-2)} & \dots & & \\ \dots & r^{(1)} & r^{(0)} & r^{(-1)} & \dots & & \\ \dots & r^{(2)} & r^{(1)} & r^{(0)} & \dots & & \\ & \vdots & \vdots & \vdots & & & \end{pmatrix}. \quad (3.58)$$

The prescription for the dispersion relation is the same as that for the case of the neutral components. Firstly, we choose an integer n from the Brillouin zone $-N/2 < n \leq N/2$. Then we diagonalize the matrix $E^{(n)}$ and find the eigenvalue $\bar{\omega}_{(n,j)}$ and the eigenvector $\mathbf{g}_+^{(n,j)}$. In order to do this by numerical computations, we have to truncate the infinitely large matrix $E^{(n)}$ to be a finite one $\tilde{E}^{(n)}$ whose size is $(2\Lambda + 1)^2$ as before.

Now, we have completed all necessary preparations for numerically obtaining the dispersion relations for any CSL backgrounds.

3.2 The noninteractive case of $\epsilon = 0$ and $\beta = 0$

First, let us consider the noninteractive case of $\epsilon = 0$ and $\beta = 0$. Eqs. (3.12) and (3.46) become

$$(-\partial_{\zeta}^2 + \cos \bar{\phi}_{\pm}) \varphi_{\pm}^{(n)} = m_{(n)}^2 \varphi_{\pm}^{(n)}, \quad (3.59)$$

$$(-\partial_{\zeta}^2 - (\bar{\phi}_3')^2 + \cos \bar{\phi}_0 \cos \bar{\phi}_3) \psi_+^{(n)} = \mu_{(n)}^2 \psi_+^{(n)}. \quad (3.60)$$

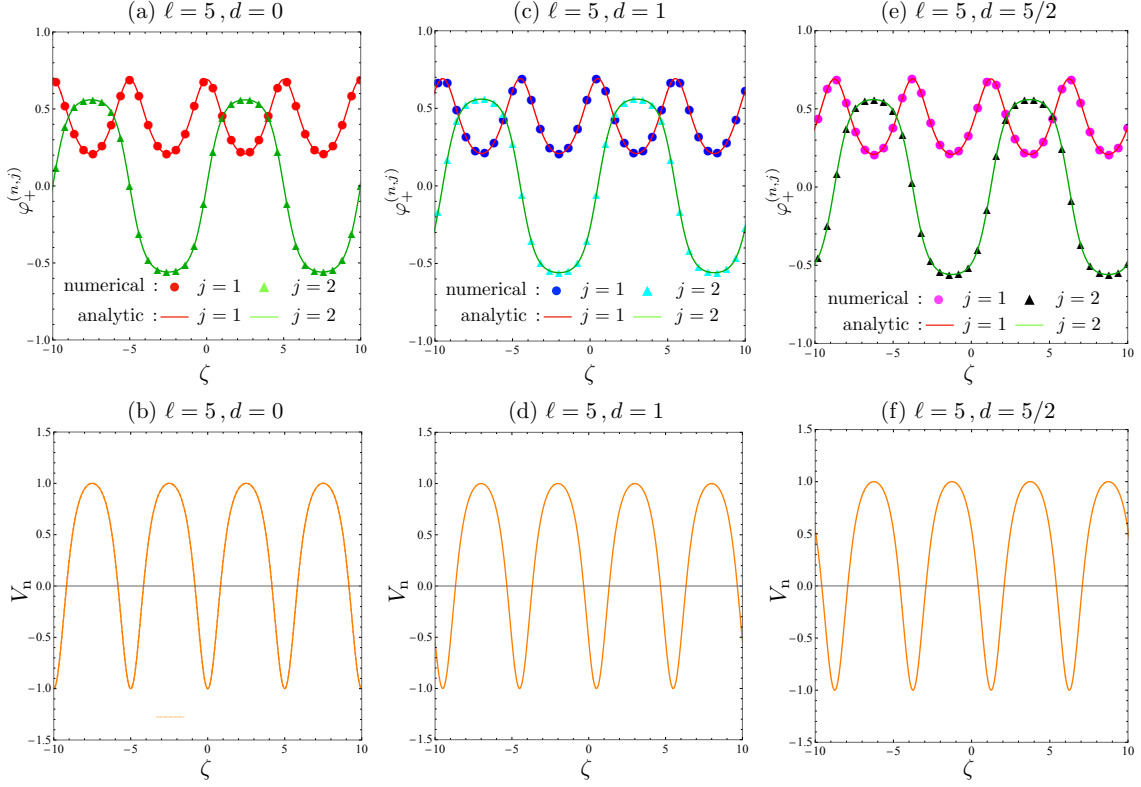


Figure 5. [The noninteractive case: the neutral components $\varphi_+^{(n,j)}$] In the top row, $\varphi_+^{(0,1)}$ for $d = 0, 1, 5/2$ are shown by the red, blue, and magenta-filled circles, respectively. $\varphi_+^{(\pi/\ell, 2)}$ for $d = 0, 1, 5/2$ are also shown by the green, cyan and black-filled triangles, respectively. The solid curves are the analytic results given in eqs. (3.66) and (3.72). In the bottom row, the potentials V_n for $d = 0, 1, 5/2$ are shown.

In order to avoid a confusion in notations, we have denoted $\bar{\omega}_{(n)} \rightarrow m_{(n)}$ for $\varphi_{\pm}^{(n)}$, and $\bar{\omega}_{(n)} \rightarrow \mu_{(n)}$ for $\psi_{\pm}^{(n)}$. The background configuration is given by

$$\bar{\phi}_{\pm} = 2 \operatorname{am} \left(\frac{\zeta \mp d/2}{k}, k \right) + \pi. \quad (3.61)$$

d is the relative distance between the up and down solitons which is a free parameter since there is no interaction between the up and down CSLs at $\epsilon = 0$ and $\beta = 0$. This case is particularly simple since φ_+ and φ_- are decoupled. Inserting these solutions into the potential parts of eqs. (3.59) and (3.60), we get

$$\cos \bar{\phi}_{\pm} = 2 \operatorname{sn}_{\pm}^2 - 1 \equiv V_n, \quad (3.62)$$

$$-(\bar{\phi}'_3)^2 + \cos \bar{\phi}_0 \cos \bar{\phi}_3 = -\frac{1}{k^2} (\operatorname{dn}_+ - \operatorname{dn}_-)^2 - \operatorname{cn}_+^2 \operatorname{cn}_-^2 + \operatorname{sn}_+^2 \operatorname{sn}_-^2 \equiv V_c, \quad (3.63)$$

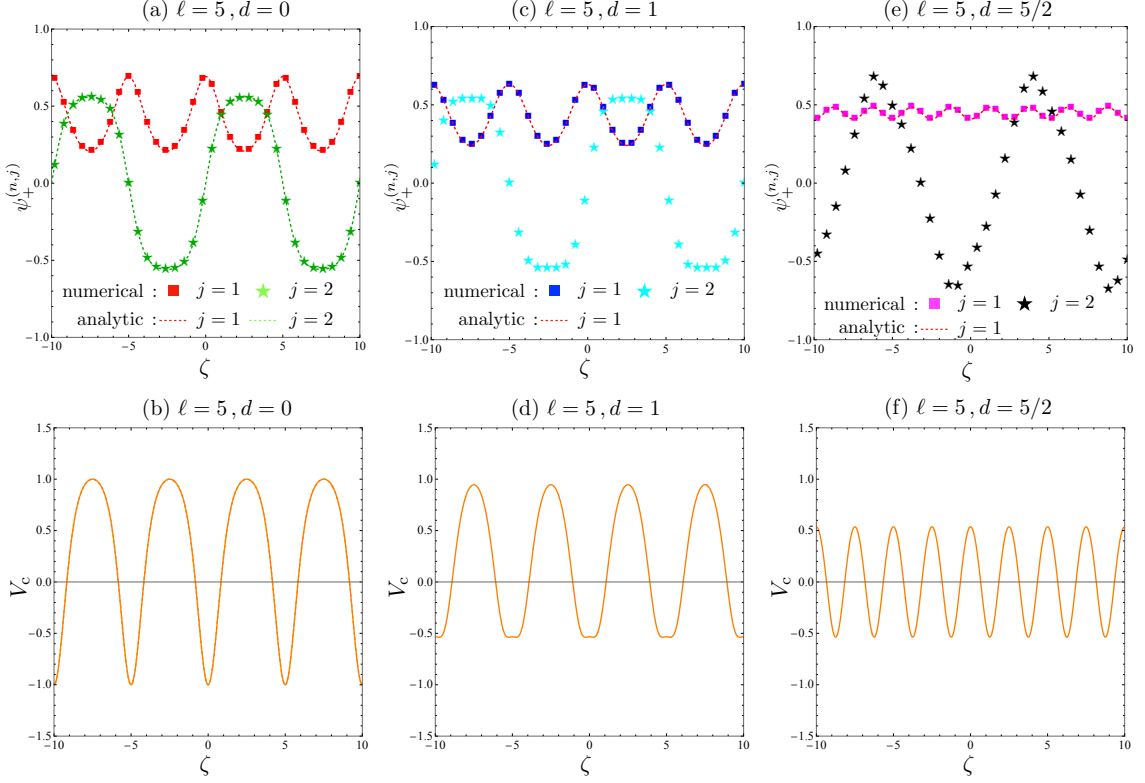


Figure 6. [Noninteracting case: the charged components $\psi_+^{(n,j)}$] In the top row, $\psi_+^{(0,1)}$ for $d = 0, 1, 5/2$ are shown by the red, blue, and magenta-filled squares, respectively. $\psi_+^{(\pi/\ell, 2)}$ for $d = 0, 1, 5/2$ are also shown by the green, cyan, and black-filled stars, respectively. The analytic solution in eq. (3.67) of $\psi_+^{(0,1)}$ for all $d = 0, 1, 5/2$ corresponds to the red-dotted lines. The analytic solution of $\psi_+^{(\pi/\ell, 2)}$ is only known for the case $d = 0$, which is shown by the green dotted line in (a). In the bottom row, the potentials V_c for $d = 0, 1, 5/2$ are shown.

where we have defined $\text{sn}_\pm = \text{sn}((\zeta \mp d/2)/k, k)$, $\text{cn}_\pm = \text{cn}((\zeta \mp d/2)/k, k)$ and $\text{dn}_\pm = \text{dn}((\zeta \mp d/2)/k, k)$ for short. Thus, eqs. (3.59) and (3.60) read

$$\left(-\frac{d^2}{d\zeta^2} + 2\text{sn}_\pm^2 - 1\right)\varphi_\pm^{(n,j)} = m_{(n,j)}^2\varphi_\pm^{(n,j)}, \quad (3.64)$$

$$\left[-\frac{d^2}{d\zeta^2} - \frac{1}{k^2}(\text{dn}_+ - \text{dn}_-)^2 - \text{cn}_+^2\text{cn}_-^2 + \text{sn}_+^2\text{sn}_-^2\right]\psi_+^{(n,j)} = \mu_{(n,j)}^2\psi_+^{(n,j)}. \quad (3.65)$$

Here, we manifestly show the band index j for labeling the eigenvalues $m_{(n,j)}$ and $\mu_{(n,j)}$ with the fixed n .

Note that the cases of $d = 0$ and $d \neq 0$ are qualitatively different. Since $\phi_+ = \phi_- = \phi_0$ ($\phi_3 = 0$) in the former case, φ_\pm and ψ_+ satisfy the identical equation. On the other hand, in the latter case, the neutral components $\varphi_\pm^{(n)}$ satisfy the obviously different equation from those for the charged components $\psi_+^{(n)}$. Regardless of d , we can analytically show that the

lowest eigenstates for $n = 0$ (corresponding to $\bar{p} = 0$) and $j = 1$ are massless as

$$m_{(0,1)}^2 = 0, \quad \varphi_{\pm}^{(0,1)} = \frac{1}{\sqrt{N^{(0,1)}}} \operatorname{dn} \left(\frac{\zeta \mp d/2}{k}, k \right), \quad (3.66)$$

$$\mu_{(0,1)}^2 = 0, \quad \psi_{+}^{(0,1)} = \frac{1}{\sqrt{M^{(0,1)}}} \left[\operatorname{dn} \left(\frac{\zeta - d/2}{k}, k \right) + \operatorname{dn} \left(\frac{\zeta + d/2}{k}, k \right) \right], \quad (3.67)$$

where $N^{(0,1)}$ and $M^{(0,1)}$ are normalization factors defined as

$$N^{(0,1)} = \int_0^{\ell} d\zeta \operatorname{dn} \left(\frac{\zeta \mp d/2}{k}, k \right)^2 = 2kE(k), \quad (3.68)$$

$$M^{(0,1)} = \int_0^{\ell} d\zeta \left[\operatorname{dn} \left(\frac{\zeta - d/2}{k}, k \right) + \operatorname{dn} \left(\frac{\zeta + d/2}{k}, k \right) \right]^2. \quad (3.69)$$

In figure 5 and 6, we show these zero modes given in eqs. (3.66) and (3.67). They are localized at the potential minima of V_n and V_c , respectively. There are always four massless modes. Their physical interpretations depend on d . When $d = 0$, the background configuration is the Abelian CSL ($\phi_{1,2,3} = 0$) which is invariant under $SU(2)_V$. One of the four zero modes is the translational zero mode, whereas the other three are members of the triplet and are the so-called quasi-NG modes [67, 68] behind which there are no spontaneously broken symmetries. When $d \neq 0$, the background configuration is the non-Abelian CSL ($\phi_3 \neq 0$). Then, $\varphi_{\pm}^{(0)}$ are the phonons propagating independently on the u- and d-CSLs, corresponding to the spontaneously broken translational symmetries. Precisely speaking, the genuine translational zero mode is unique, and the rest is the quasi-NG mode related to the relative motion of the u- and d-CSLs. On the other hand, $\psi_{\pm}^{(0)}$ is the massless modes associated with the SSB $SU(2)_V \rightarrow U(1)$, which is called the isospinon [42]. In both cases of $d = 0$ and $d \neq 0$, the total number of zero modes are preserved [67].

Next, let us include a nonzero crystal momentum \bar{p} and determine the dispersion relation. The results from the numerical calculations are shown in figure 7 for the three different separations $d = 0, 1, 5/2$ for $\ell = 5$ ($d = 0$ is the closest case and $d = 5/2$ is the farthest case). In fact, eq. (3.64) for the neutral components (phonons) can be analytically solved as follows. It is the so-called Lamé equation [66] which can be solved by using the Jacobi theta functions. For $N = \infty$ (continuum limit), the solution for $j = 1$ (called the valence band) is

$$\bar{p} = Z(\alpha, k') + \frac{\pi\alpha}{2KK'}, \quad m_{(\bar{p},1)}^2 = \frac{k'^2}{k^2} \operatorname{sn}^2(\alpha, k'), \quad (3.70)$$

where α is an arbitrary real number, and Z is the Jacobi Zeta function.⁴ Here, we defined $k' = \sqrt{1 - k^2}$ and $K' = K(k')$. In a manner similar to the above, the solution for $j = 2$ (called the conduction band) is given as

$$\bar{p} = \frac{\pi\alpha}{2KK'} + Z(\alpha, k') + \operatorname{dn}(\alpha, k') \frac{\operatorname{cn}(\alpha, k')}{\operatorname{sn}(\alpha, k')}, \quad m_{(\bar{p},2)}^2 = \frac{1}{k^2 \operatorname{sn}^2(\alpha, k')}. \quad (3.71)$$

⁴The definition of the Jacobi zeta function is $Z(\alpha, k) = E_k(\alpha) - \frac{E(k)}{K(k)}\alpha$, with $E_k(\alpha) = \int_0^{\alpha} d\alpha' \operatorname{dn}^2(\alpha', k)$.

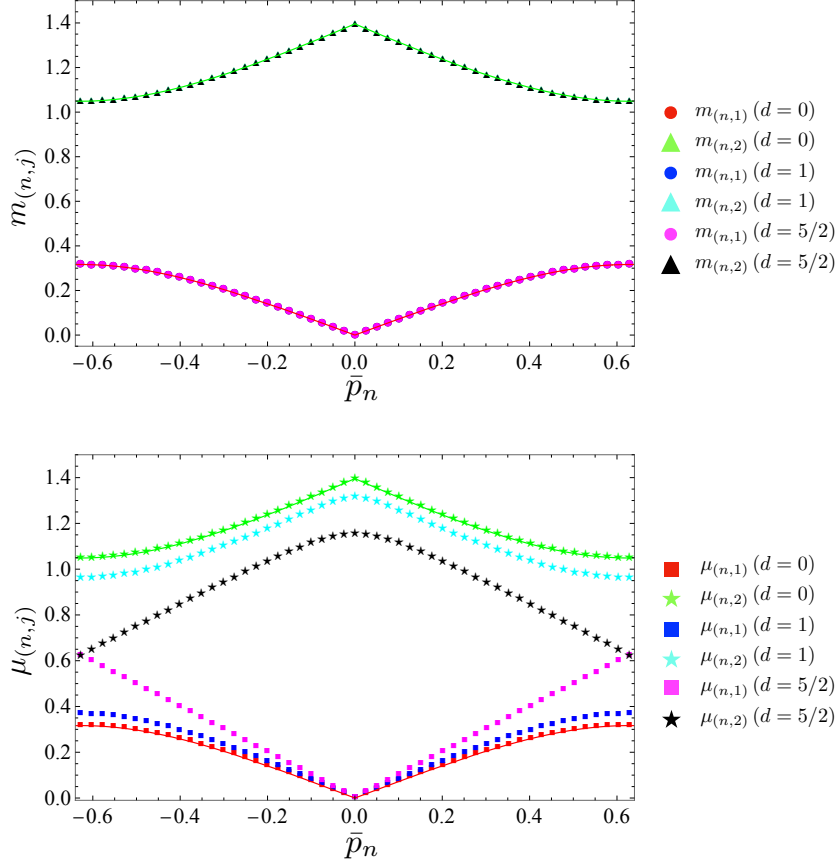


Figure 7. [Noninteracting case] Dispersion relations of the phonons $\varphi_+^{(n,j)}$ (upper panel) and the isospinons $\psi_+^{(n,j)}$ (bottom panel) for the background CSL with $\ell = 5$. In the upper panel, the $j = 1$ ($j = 2$) modes at $d = 0, 1, 5/2$ are indicated by red (green), blue (cyan), and magenta (black) circles (triangles), respectively. The solid red (green) curves correspond to the analytic solution in eq. (3.70) [(3.71)]. All three circles (triangles) with different colors completely overlap, reflecting the fact eq. (3.59) is independent of d . In the bottom panel, the $j = 1$ ($j = 2$) modes at $d = 0, 1, 5/2$ are shown by red (green), blue (cyan), and magenta (black) squares (stars), respectively. The dispersion relation of the isospinon for $d = 0$ coincides with the one for the phonon. Consequently, the red squares and the green stars are on the solid red and green curves, respectively.

The lowest energy solution for $j = 2$ is at the edge of the first Brillouin zone $\bar{p} = \pi/\ell$ and it is analytically given by

$$\varphi_{\pm}^{(\pi/\ell,2)} = \frac{1}{\sqrt{N(\pi/\ell,2)}} \operatorname{sn} \left(\frac{\zeta \mp d/2}{k}, k \right), \quad (3.72)$$

$$N(\pi/\ell,2) = \int_0^\ell d\zeta \operatorname{sn} \left(\frac{\zeta \mp d/2}{k}, k \right)^2 = \frac{2(K(k) - E(k))}{k}. \quad (3.73)$$

We compare the numerical and analytical dispersion relations for the neutral components in the top panel of fig. 7. They nicely agree with each other. Note that eq. (3.64) is independent of d , so that the dispersion relations for $d = 0, 1, 5/2$ completely overlap. The

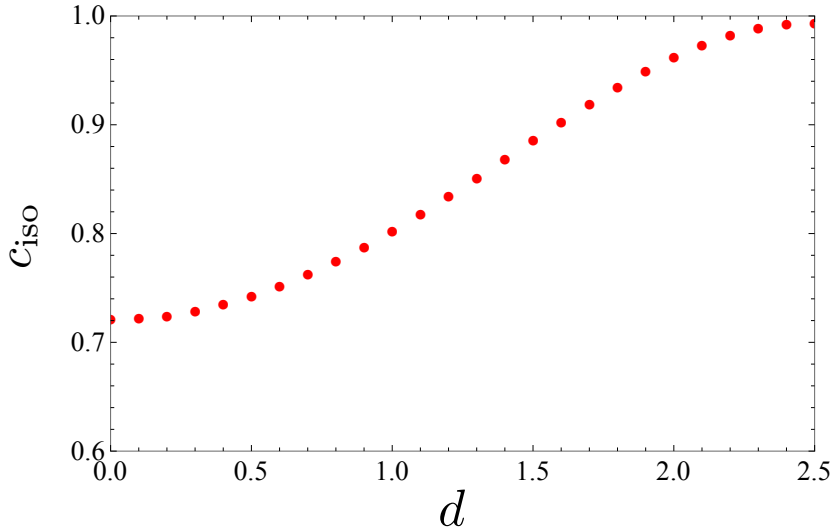


Figure 8. The d -dependence of the group velocity of the isospinon at $\bar{p} = 0$ for $\ell = 0$, $\epsilon = 0$ and $\beta = 0$.

phonon group velocities are known to be [69]

$$c_{\text{ph}}^{(\text{u,d})} = \sqrt{1 - k^2} \frac{E(k)}{K(k)}. \quad (3.74)$$

This vanishes at the single soliton limit with $k = 1$ ($B = B_{\text{CSL}}$) whereas the rapidity approaches the speed of light as $k \rightarrow 0$ ($B \rightarrow \infty$) [9]. This behavior agrees with the intuition that the lattice size is 0 and the CSL is maximally hard at $k = 0$ whereas the lattice size is infinite and the CSL is maximally soft at $k = 1$.

In contrast, the eigen equation (3.65) for the charged components (isospinons) for $0 < d \leq \ell/2$ cannot be solved analytically, we solve it numerically for the first time to the best of our knowledge. The results are shown in the bottom panel of fig. 7. Only when $d = 0$, eq. (3.65) is identical to eq. (3.64), which can be analytically solved as explained above. The red squares and green stars in the bottom panel of fig. 7 show the dispersion relations for $j = 1$ and $j = 2$ of the Abelian CSL ($d = 0$). The dispersion relations of the dimer CSL ($d = 1$) are shown by the blue squares ($j = 1$) and cyan stars ($j = 2$). Similarly, those of the deconfined CSL ($d = 5/2$) correspond to the magenta squares ($j = 1$) and black stars ($j = 2$). Interestingly, the gap between $j = 1$ and $j = 2$ bands at the edge of the first Brillouin zone $\bar{p} = \pi/\ell$ gradually narrows as increasing the separation d , and it closes at $d = \ell/2 = 5/2$ (the black stars and magenta squares). Furthermore, the dispersion relation of the isospinon at $d = \ell/2$ looks linear and its group velocity seems to reach at the speed of light. This implies that the deconfined CSL ($d = \ell/2$) is the hardest limit for the isospinons. The d dependence of the group velocity of the isospinon at $\bar{p} = 0$ is shown in fig. 8. Note that the group velocity is usually defined as the momentum derivative of the dispersion relation. However, since the dispersion relation is currently calculated only for discrete momenta \bar{p}_n , the group velocity was numerically computed using forward

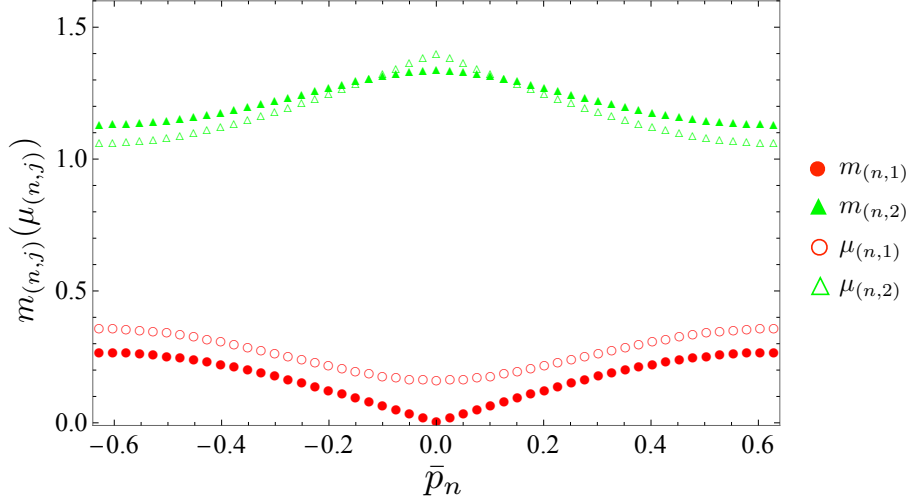


Figure 9. [Interacting case] Dispersion relation of $\varphi_{1,2,3}$ and φ_0 in eqs. (3.76) and (3.77) for $\epsilon = 0$, $\beta = \pi/16$ and $\ell = 5$. The red-(un)filled circles are the $j = 1$ modes of φ_0 ($\varphi_{1,2,3}$). The green-(un)filled triangles are the $j = 2$ modes of φ_0 ($\varphi_{1,2,3}$).

difference:

$$c_{\text{iso}} \equiv \frac{\mu_{(n+1,j)} - \mu_{(n,j)}}{\Delta \bar{p}_n}, \quad \Delta \bar{p}_n \equiv \frac{2\pi(n+1)}{N\ell} - \frac{2\pi n}{N\ell} = \frac{2\pi}{N\ell}. \quad (3.75)$$

3.3 Confined phase

In this phase, the up and down solitons completely adhere, so the separation is $d = 0$. Then, only $\bar{\phi}_0$ spatially modulates and $\bar{\phi}_3 = 0$. We choose typical parameters for the confined phase: $\epsilon = 0, \beta = \pi/16, \ell = 5$. Here we use $\varphi_{0,1,2,3}$ instead of φ_{\pm} and ψ_{\pm} . Since the isospin symmetry $SU(2)_V$ is unbroken, $\varphi_{1,2,3}$ form the triplet of $SU(2)_V$ and they satisfy the identical equation. The EOMs of the fluctuations become

$$m_{(n,j)}^2 \varphi_0^{(n,j)} = [-\partial_{\zeta}^2 + (4 \sin \beta \cos(2\bar{\phi}_0) + \cos \beta \cos \bar{\phi}_0)] \varphi_0^{(n,j)}, \quad (3.76)$$

$$\mu_{(n,j)}^2 \varphi_{1,2,3}^{(n,j)} = [-(1 - \epsilon) \partial_{\zeta}^2 + \cos \beta \cos \bar{\phi}_0] \varphi_{1,2,3}^{(n,j)}. \quad (3.77)$$

We numerically solve these equations, and their dispersion relations are shown in figure 9. Comparing this with the top panel of figure 7, we find only one phonon in $\varphi_0^{(n,1)}$ which corresponds to the translational zero mode. The other phonon in $\varphi_3^{(n,1)}$ at $\epsilon = \beta = 0$, which is the quasi-NG, is lifted due to the attractive interaction between the up- and down-CSLs. Because of the isospin symmetry $SU(2)_V$, $\varphi_{1,2}$ has the same dispersion relation as φ_3 . The phonon $\varphi_0^{(n,1)}$ dispersion relation corresponds to the red-filled circle in figure 9, whereas the red-unfilled one to the lifted quasi-NG mode $\varphi_{1,2,3}^{(n,1)}$.

3.4 Deconfined phase

The up and down solitons in the deconfined phase are maximally separated; namely, the separation is $d = \ell/2$. The spatial translational symmetry is spontaneously broken in

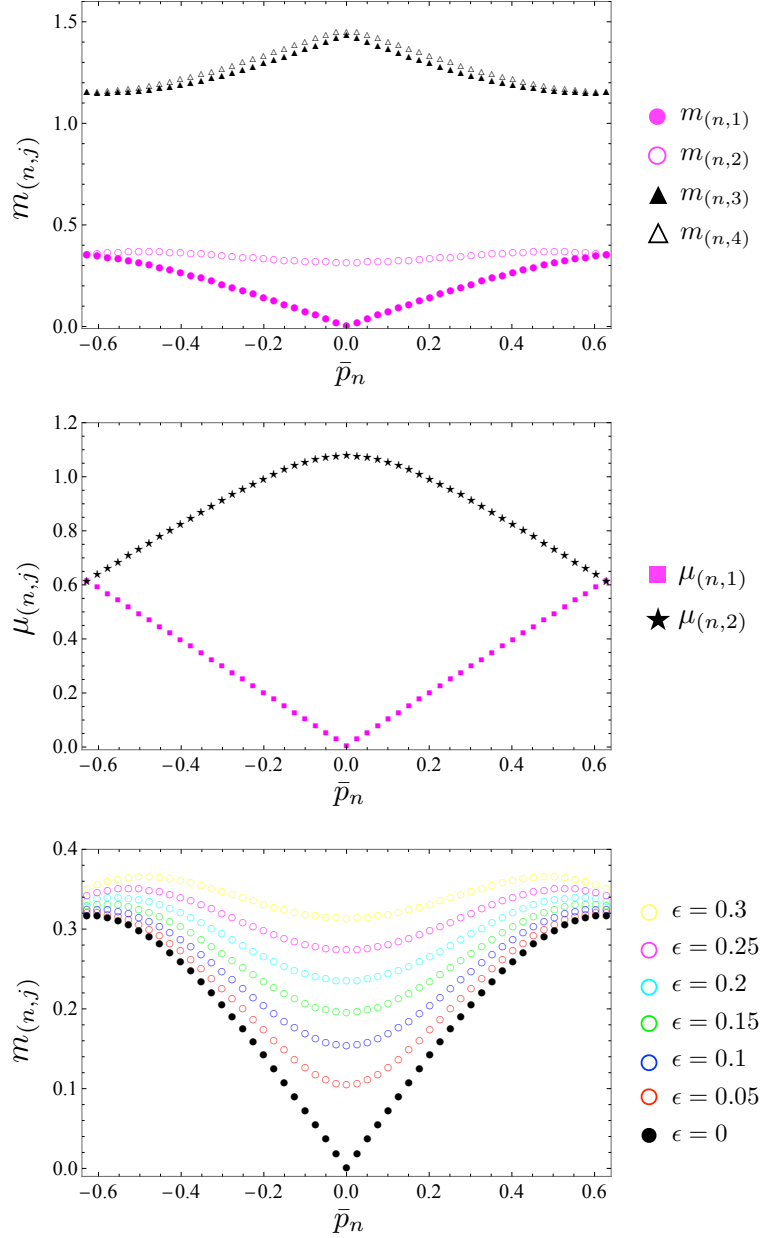


Figure 10. [Interacting case] Dispersion relation of the neutral components $\varphi_{\pm}^{(n,j)}$ (upper panel) and charged components $\psi_{\pm}^{(n,j)}$ (middle panel) for $\epsilon = 0.3$, $\beta = 0$ and $\ell = 5$. In the upper panel, we show the low-lying four bands $j = 1, 2, 3, 4$. In the middle panel, we show the low-lying two bands with $j = 1, 2$ for $\psi_{\pm}^{(n,j)}$ (Each band is doubly degenerate for $+$ and $-$). In the bottom panel, the ϵ -dependence of $\bar{\omega}_{(n,2)}$ for $\epsilon = 0.05, 0.1, 0.15, 0.2, 0.25, 0.3$ with $\beta = 0$ and $\ell = 5$ being fixed is shown. The black-filled circles coincide with the magenta-filled circles in the top panel, and the yellow-unfilled circles coincide with the magenta-unfilled circles in the top panel.

the deconfined phase as well as the confined one. In contrast to the two phonons in the noninteractive case of $\epsilon = 0$ and $\beta = 0$, there appears to be only one phonon due to the

repulsive interaction between the up and down solitons.

We numerically solve eq. (3.21) for $\epsilon \neq 0$ and $\beta = 0$ yielding a CSL in the deconfined phase. Note that, when $\beta = 0$ the inter-soliton force is generated only by ϵ , and it is repulsive for any positive ϵ . The dispersion relations are summarized in figure 10.

The upper panel in figure 10 shows that the gapless phonon mode (magenta-filled circle) $\epsilon = 0.3$ appears due to the spontaneous translational symmetry breaking. The gapped mode (magenta-unfilled circle) originates from one of the two gapless phonons present when $\epsilon = 0$ and $\beta = 0$. Hence, as ϵ nears zero, the dispersion relation for this gapped mode aligns with that of $\epsilon = 0$ and $\beta = 0$ as can be seen in the bottom panel of figure 10. As for the black-filled and -unfilled triangles, they tend to be degenerate in the limit of ϵ to zero. As a result, they align with the black triangles depicted in figure 7.

In contrast to the confined phase, the deconfined phase possesses two NG modes (isospinons) resulting from the spontaneous breaking of the vector $SU(2)_V$ symmetry as illustrated in the middle panel of figure 10. The eigenvalues $\mu_{n,j}$ exhibit double degeneracy because both $\psi^{(n,j)}$ and its complex conjugate $\psi^{(n,j)*}$ adhere to the same equation. As a result, in the center panel of figure 10, the bands corresponding to $j = 1$ and $j = 2$ are degenerate. This is similar to the upper panel, where the first four eigenvalues are illustrated in ascending order.

3.5 Dimer phase

As discussed in section 2, the deconfined and dimer phases share the same pattern of continuous symmetry breaking, with their only distinction lying in the discrete symmetry. Consequently, the emergence of a single phonon and two isospinons in the dimer phase is naturally expected.

We again numerically solve equations (3.21) and (3.55) for $\epsilon = 0.1$ and $\epsilon = 0.15$. The lattice constant is again fixed to be $\ell = 5$, and we now turn on $\beta = \pi/16$. We numerically verified the emergence of a single phonon, resulting from the spontaneous breaking of spatial translational symmetry, which is depicted by the blue-filled circles in (a) and (c) of figure 11. We also confirmed the presence of two isospinons, as indicated by the blue-filled squares in (b) and (d) of figure 11. These are comparable to those observed in the top and middle panels of figure 10 for the deconfined phase. A notable distinction, however, is evident at the edge of the Brillouin zone ($\bar{p}_n = \pm\pi/\ell$). The two bands with $j = 1$ and $j = 2$ close there in the deconfined case whereas there is a finite gap for the dimer case. Comparing (b) and (d) in figure 11, it clearly shows that the band gap narrows as ϵ increases. This can be understood as follows. When we increase ϵ , the repulsion between the up and down solitons becomes stronger, so that the dimer becomes longer. Consequently, at some critical ϵ , the transition from the dimer phase to the deconfined phase occurs. We have seen a similar phenomenon for $\epsilon = 0$ and $\beta = 0$, as demonstrated in the bottom panel of figure 7, where the band gap narrows as d increases.

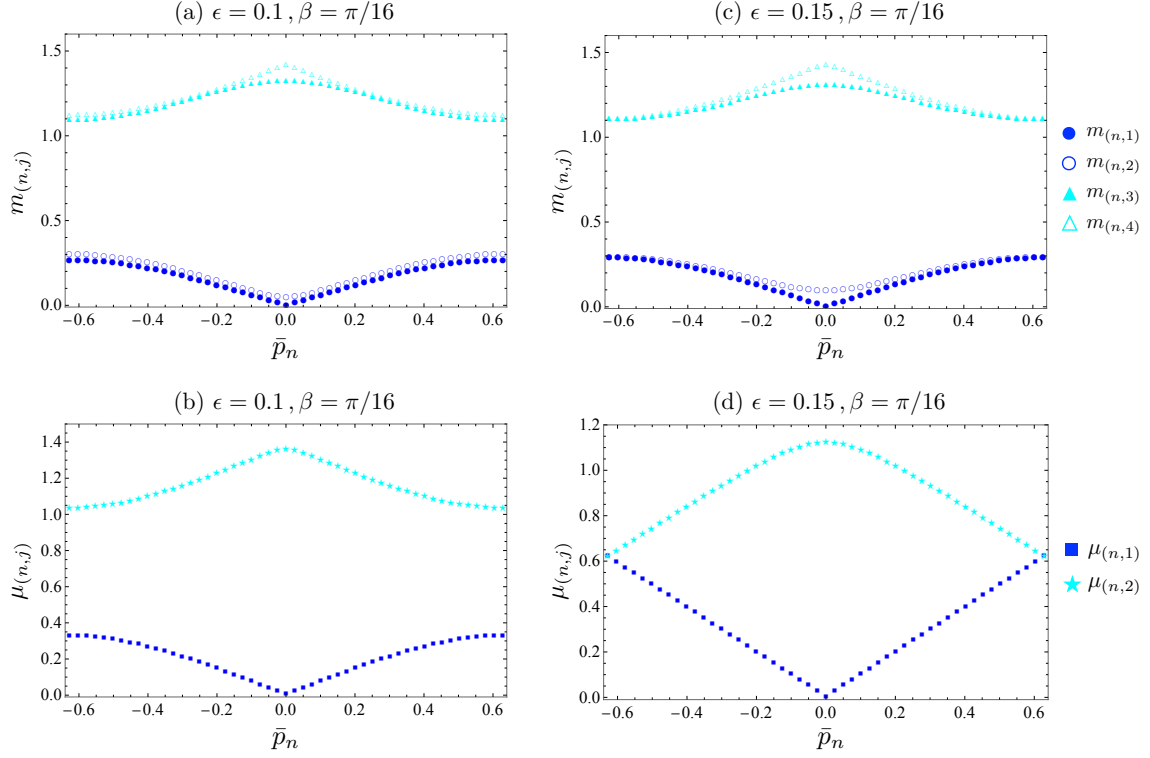


Figure 11. Dispersion relation of $\varphi_{\pm}^{(n,j)}$ and $\psi_{\pm}^{(n,j)}$ in the dimer phase. For $\epsilon = 0.1$ and $\beta = \pi/16$, the dispersion relations of $\varphi_{\pm}^{(n,j)}$ and $\psi_{\pm}^{(n,j)}$ are (a) and (b), respectively. For $\epsilon = 0.15$ and $\beta = \pi/16$, the dispersion relations of $\varphi_{\pm}^{(n,j)}$ and $\psi_{\pm}^{(n,j)}$ are (c) and (d), respectively.

4 Summary and discussion

We have numerically studied excitations and their dispersion relations around Abelian and non-Abelian CSLs in the confined, deconfined, and dimer phases of rapidly rotating QCD matter. We have found three gapless type-A NG modes with linear dispersion relations: two isospinons (the $\mathbb{C}P^1$ modes) and a phonon corresponding to the spontaneously broken vector $SU(2)_V$ and translational symmetries in non-Abelian CSLs (deconfined and dimer phases). We also have found only one gapless NG mode (a phonon) in the confined phase since the $SU(2)_V$ symmetry is recovered. We have obtained gapped modes (first excited modes) as well in these phases. The number of gapless NG modes is different between Abelian (η) and non-Abelian CSLs while those cannot distinguish the two non-Abelian CSLs, the deconfined and dimer phases since they are distinct only in terms of the discrete symmetry. We also have found in the deconfined phase that the dispersion relation of the isospinons becomes of the Dirac type, *i. e.* linear even at large momentum.

Here, we address some discussions. The first is about the types of NG modes. In the non-Abelian CSLs, the $\mathbb{C}P^1$ modes of neighboring solitons repel and are antialigned at least in the parameters that we studied. Thus, they behave as an anti-ferromagnetic Heisenberg model. It is an open question whether there is the case that the $\mathbb{C}P^1$ modes of neighboring

solitons attract each other and tend to be aligned, constructing a soliton lattice behaving as a ferromagnet. This question is related to the type of NG modes; In such a case, the $\mathbb{C}P^1$ modes would be of type-B with a quadratic dispersion relation. In this regard, type-B NG modes often appear in finite density systems which are nonrelativistic. For instance, in the presence of a single domain wall in the nonrelativistic $\mathbb{C}P^1$ model, the translational zero mode is coupled with an internal mode to become a type-B NG mode [70, 71].⁵ Whether type-B NG modes can appear in a CSL is one of the directions to explore.

In this paper, we have not considered a coupling to the electromagnetism. When the electromagnetic coupling is taken into account which is more relevant to the case of neutron stars and heavy-ion collisions, a photon has quadratic dispersion relation (as a type-B NG mode) [74]. Such nonrelativistic photon should be discussed in a non-Abelian CSL background.

The extension to the three-flavor case (the up, down, and strange quarks) is one of the important directions. In this case, the η' meson has the anomalous coupling with rotation, and the Abelian η' -CSL was studied before [40]. In some parameter regions, a single η' -soliton is split into three non-Abelian solitons (the deconfined phase). In such a case, the vector symmetry $SU(3)_V$ is spontaneously broken to an $SU(2) \times U(1)$ subgroup in the vicinity of each non-Abelian soliton so that there appear $\mathbb{C}P^2 \simeq SU(3)_V/[SU(2) \times U(1)]$ zero modes localized around each soliton. If the $\mathbb{C}P^2$ modes of neighboring solitons repel as the case of two flavors in the deconfined phase, then the lattice can be regarded as an antiferromagnetic $SU(3)$ Heisenberg model. A continuum limit for extremely rapid rotation would result in an $SU(3)/U(1)^2$ flag manifold nonlinear sigma model. Thus, we expect six type-A NG modes and one phonon in the three-flavor case.

CSL phases (also called spiral phases) are also present in chiral magnets accompanied by the Dzyaloshinskii-Moriya (DM) interaction [75, 76], and have been paid great attention [77–83]. Let us discuss the similarities and differences between the CSL phases in rotating QCD matter studied in this paper and those in chiral magnets. In the former, we have found isospinons ($\mathbb{C}P^2$ modes) besides a phonon, and these modes are decoupled from each other. On the other hand, in the case of chiral magnets, each domain wall or soliton carries a $U(1)$ modulus in contrast to $\mathbb{C}P^2$ moduli for the CSLs in rotating QCD matter. Thus, a soliton lattice is the XY model rather than a Heisenberg model in the CSLs in rotating QCD matter. If the potential is an easy-axis potential, the $U(1)$ moduli of the domain walls are alternate in the ground state, and so the XY model is antiferromagnetic. In the CSL, there should be a magnon corresponding to the $U(1)$ symmetry breaking beside a phonon corresponding to translational symmetry breaking. However, the $U(1)$ magnon and phonon are coupled nontrivially due to the DM interaction [84, 85], unlike the case of the CSL in the QCD matter in which case the $\mathbb{C}P^2$ isospinons and phonon are decoupled. Therefore, their type of NG bosons and dispersion relations are quite nontrivial problems to be explored in the future.

⁵It is also known that in the presence of a soliton, translational modes of the soliton sometimes can have fractional dispersion relations [72, 73]. This seems to be the case that zero modes are nonnormalizable and is not applied to CSLs.

In a different context, a lattice of non-Abelian vortices accompanied with $\mathbb{C}P^{N-1}$ modes was studied [86] instead of the non-Abelian sine-Gordon solitons considered in this paper. As in the case of non-Abelian CSLs, the interaction between neighboring vortices intermediates the propagation of the $\mathbb{C}P^{N-1}$ modes into two transverse directions of the lattice in addition to a phonon called the Tkachenko mode [61–64]. In ref. [86], a continuum limit of the lattice was studied at a large distance to yield an anisotropic $\mathbb{C}P^{N-1}$ model. Such a continuum limit should be considered for a non-Abelian CSL in QCD matter as well to yield an anisotropic $\mathbb{C}P^{N-1}$ model.

Acknowledgments

This work is supported in part by JSPS KAKENHI [Grants No. JP21H01084 (KN), and No. JP22H01221 (ME and MN)] and the WPI program “Sustainability with Knotted Chiral Meta Matter (SKCM²)” at Hiroshima University (KN and MN).

References

- [1] K. Fukushima and T. Hatsuda, *The phase diagram of dense QCD*, *Rept. Prog. Phys.* **74** (2011) 014001 [[1005.4814](#)].
- [2] S. Scherer and M. R. Schindler, *A Primer for Chiral Perturbation Theory*, vol. 830. 2012, [10.1007/978-3-642-19254-8](#).
- [3] S. K. Bogner, R. J. Furnstahl and A. Schwenk, *From low-momentum interactions to nuclear structure*, *Prog. Part. Nucl. Phys.* **65** (2010) 94 [[0912.3688](#)].
- [4] D. T. Son and A. R. Zhitnitsky, *Quantum anomalies in dense matter*, *Phys. Rev. D* **70** (2004) 074018 [[hep-ph/0405216](#)].
- [5] D. T. Son and M. A. Stephanov, *Axial anomaly and magnetism of nuclear and quark matter*, *Phys. Rev. D* **77** (2008) 014021 [[0710.1084](#)].
- [6] J. Goldstone and F. Wilczek, *Fractional Quantum Numbers on Solitons*, *Phys. Rev. Lett.* **47** (1981) 986.
- [7] E. Witten, *Global Aspects of Current Algebra*, *Nucl. Phys. B* **223** (1983) 422.
- [8] M. Eto, K. Hashimoto and T. Hatsuda, *Ferromagnetic neutron stars: axial anomaly, dense neutron matter, and pionic wall*, *Phys. Rev. D* **88** (2013) 081701 [[1209.4814](#)].
- [9] T. Brauner and N. Yamamoto, *Chiral Soliton Lattice and Charged Pion Condensation in Strong Magnetic Fields*, *JHEP* **04** (2017) 132 [[1609.05213](#)].
- [10] T.-G. Lee, E. Nakano, Y. Tsue, T. Tatsumi and B. Friman, *Landau-Peierls instability in a Fulde-Ferrell type inhomogeneous chiral condensed phase*, *Phys. Rev. D* **92** (2015) 034024 [[1504.03185](#)].
- [11] Y. Hidaka, K. Kamikado, T. Kanazawa and T. Noumi, *Phonons, pions and quasi-long-range order in spatially modulated chiral condensates*, *Phys. Rev. D* **92** (2015) 034003 [[1505.00848](#)].
- [12] T. Brauner and S. V. Kadam, *Anomalous low-temperature thermodynamics of QCD in strong magnetic fields*, *JHEP* **11** (2017) 103 [[1706.04514](#)].

- [13] G. W. Evans and A. Schmitt, *Chiral anomaly induces superconducting baryon crystal*, *JHEP* **09** (2022) 192 [2206.01227].
- [14] G. W. Evans and A. Schmitt, *Chiral Soliton Lattice turns into 3D crystal*, 2311.03880.
- [15] M. Eto, K. Nishimura and M. Nitta, *How baryons appear in low-energy QCD: Domain-wall Skyrmion phase in strong magnetic fields*, 2304.02940.
- [16] M. Eto, K. Nishimura and M. Nitta, *Phase diagram of QCD matter with magnetic field: domain-wall Skyrmion chain in chiral soliton lattice*, *JHEP* **12** (2023) 032 [2311.01112].
- [17] M. Kawaguchi, Y.-L. Ma and S. Matsuzaki, *Chiral soliton lattice effect on baryonic matter from a skyrmion crystal model*, *Phys. Rev. C* **100** (2019) 025207 [1810.12880].
- [18] S. Chen, K. Fukushima and Z. Qiu, *Skyrmions in a magnetic field and $\pi 0$ domain wall formation in dense nuclear matter*, *Phys. Rev. D* **105** (2022) L011502 [2104.11482].
- [19] S. Chen, K. Fukushima and Z. Qiu, *Magnetic enhancement of baryon confinement modeled via a deformed Skyrmion*, *Phys. Lett. B* **843** (2023) 137992 [2303.04692].
- [20] T. Brauner and S. Kadam, *Anomalous electrodynamics of neutral pion matter in strong magnetic fields*, *JHEP* **03** (2017) 015 [1701.06793].
- [21] T. Brauner, H. Kolešová and N. Yamamoto, *Chiral soliton lattice phase in warm QCD*, *Phys. Lett. B* **823** (2021) 136767 [2108.10044].
- [22] T. Brauner and H. Kolešová, *Chiral soliton lattice at next-to-leading order*, *JHEP* **07** (2023) 163 [2302.06902].
- [23] M. Eto and M. Nitta, *Quantum nucleation of topological solitons*, *JHEP* **09** (2022) 077 [2207.00211].
- [24] T. Higaki, K. Kamada and K. Nishimura, *Formation of a chiral soliton lattice*, *Phys. Rev. D* **106** (2022) 096022 [2207.00212].
- [25] Z. Qiu and M. Nitta, *Quasicrystals in QCD*, *JHEP* **05** (2023) 170 [2304.05089].
- [26] STAR collaboration, *Global Λ hyperon polarization in nuclear collisions: evidence for the most vortical fluid*, *Nature* **548** (2017) 62 [1701.06657].
- [27] STAR collaboration, *Global polarization of Λ hyperons in Au+Au collisions at $\sqrt{s_{NN}} = 200$ GeV*, *Phys. Rev. C* **98** (2018) 014910 [1805.04400].
- [28] H.-L. Chen, K. Fukushima, X.-G. Huang and K. Mameda, *Analogy between rotation and density for Dirac fermions in a magnetic field*, *Phys. Rev.* **D93** (2016) 104052 [1512.08974].
- [29] S. Ebihara, K. Fukushima and K. Mameda, *Boundary effects and gapped dispersion in rotating fermionic matter*, *Phys. Lett.* **B764** (2017) 94 [1608.00336].
- [30] Y. Jiang and J. Liao, *Pairing Phase Transitions of Matter under Rotation*, *Phys. Rev. Lett.* **117** (2016) 192302 [1606.03808].
- [31] M. N. Chernodub and S. Gongyo, *Interacting fermions in rotation: chiral symmetry restoration, moment of inertia and thermodynamics*, *JHEP* **01** (2017) 136 [1611.02598].
- [32] M. N. Chernodub and S. Gongyo, *Effects of rotation and boundaries on chiral symmetry breaking of relativistic fermions*, *Phys. Rev.* **D95** (2017) 096006 [1702.08266].
- [33] Y. Liu and I. Zahed, *Rotating Dirac fermions in a magnetic field in 1+2 and 1+3 dimensions*, *Phys. Rev. D* **98** (2018) 014017 [1710.02895].

- [34] H. Zhang, D. Hou and J. Liao, *Mesonic Condensation in Isospin Matter under Rotation*, *Chin. Phys. C* **44** (2020) 111001 [[1812.11787](#)].
- [35] L. Wang, Y. Jiang, L. He and P. Zhuang, *Local suppression and enhancement of the pairing condensate under rotation*, *Phys. Rev. C* **100** (2019) 034902 [[1901.00804](#)].
- [36] H.-L. Chen, X.-G. Huang and K. Mameda, *Do charged pions condense in a magnetic field with rotation?*, [1910.02700](#).
- [37] M. N. Chernodub, *Inhomogeneous confining-deconfining phases in rotating plasmas*, *Phys. Rev. D* **103** (2021) 054027 [[2012.04924](#)].
- [38] M. N. Chernodub, V. A. Goy and A. V. Molochkov, *Inhomogeneity of a rotating gluon plasma and the Tolman-Ehrenfest law in imaginary time: Lattice results for fast imaginary rotation*, *Phys. Rev. D* **107** (2023) 114502 [[2209.15534](#)].
- [39] X.-G. Huang, K. Nishimura and N. Yamamoto, *Anomalous effects of dense matter under rotation*, *JHEP* **02** (2018) 069 [[1711.02190](#)].
- [40] K. Nishimura and N. Yamamoto, *Topological term, QCD anomaly, and the η' chiral soliton lattice in rotating baryonic matter*, *JHEP* **07** (2020) 196 [[2003.13945](#)].
- [41] H.-L. Chen, X.-G. Huang and J. Liao, *QCD phase structure under rotation*, *Lect. Notes Phys.* **987** (2021) 349 [[2108.00586](#)].
- [42] M. Eto, K. Nishimura and M. Nitta, *Phases of rotating baryonic matter: non-Abelian chiral soliton lattices, antiferro-isospin chains, and ferri/ferromagnetic magnetization*, *JHEP* **08** (2022) 305 [[2112.01381](#)].
- [43] M. Eto, K. Nishimura and M. Nitta, *Domain-wall Skyrmion phase in a rapidly rotating QCD matter*, [2310.17511](#).
- [44] A. Vilenkin, *Macroscopic parity-violating effects: Neutrino fluxes from rotating black holes and in rotating thermal radiation*, *Phys. Rev. D* **20** (1979) 1807.
- [45] A. Vilenkin, *Quantum field theory at finite temperature in a rotating system*, *Phys. Rev. D* **21** (1980) 2260.
- [46] D. T. Son and P. Surowka, *Hydrodynamics with Triangle Anomalies*, *Phys. Rev. Lett.* **103** (2009) 191601 [[0906.5044](#)].
- [47] K. Landsteiner, E. Megias and F. Pena-Benitez, *Gravitational Anomaly and Transport*, *Phys. Rev. Lett.* **107** (2011) 021601 [[1103.5006](#)].
- [48] K. Landsteiner, E. Megias and F. Pena-Benitez, *Anomalous Transport from Kubo Formulae*, *Lect. Notes Phys.* **871** (2013) 433 [[1207.5808](#)].
- [49] K. Landsteiner, *Notes on Anomaly Induced Transport*, *Acta Phys. Polon. B* **47** (2016) 2617 [[1610.04413](#)].
- [50] M. Nitta, *Non-Abelian Sine-Gordon Solitons*, *Nucl. Phys. B* **895** (2015) 288 [[1412.8276](#)].
- [51] M. Eto and M. Nitta, *Non-Abelian Sine-Gordon Solitons: Correspondence between $SU(N)$ Skyrmions and $\mathbb{C}P^{N-1}$ Lumps*, *Phys. Rev. D* **91** (2015) 085044 [[1501.07038](#)].
- [52] M. Nitta, *Josephson junction of non-Abelian superconductors and non-Abelian Josephson vortices*, *Nucl. Phys. B* **899** (2015) 78 [[1502.02525](#)].
- [53] M. Nitta, *Josephson instantons and Josephson monopoles in a non-Abelian Josephson junction*, *Phys. Rev. D* **92** (2015) 045010 [[1503.02060](#)].

- [54] M. Nitta, *Relations among topological solitons*, *Phys. Rev. D* **105** (2022) 105006 [[2202.03929](#)].
- [55] H. Watanabe and H. Murayama, *Unified Description of Nambu-Goldstone Bosons without Lorentz Invariance*, *Phys. Rev. Lett.* **108** (2012) 251602 [[1203.0609](#)].
- [56] Y. Hidaka, *Counting rule for Nambu-Goldstone modes in nonrelativistic systems*, *Phys. Rev. Lett.* **110** (2013) 091601 [[1203.1494](#)].
- [57] H. Watanabe and H. Murayama, *Effective Lagrangian for Nonrelativistic Systems*, *Phys. Rev. X* **4** (2014) 031057 [[1402.7066](#)].
- [58] D. A. Takahashi and M. Nitta, *Counting rule of Nambu-Goldstone modes for internal and spacetime symmetries: Bogoliubov theory approach*, *Annals Phys.* **354** (2015) 101 [[1404.7696](#)].
- [59] H. Watanabe, *Counting Rules of Nambu-Goldstone Modes*, *Ann. Rev. Condensed Matter Phys.* **11** (2020) 169 [[1904.00569](#)].
- [60] A. J. Beekman, L. Rademaker and J. van Wezel, *An Introduction to Spontaneous Symmetry Breaking*, *SciPost Phys. Lect. Notes* **11** (2019) 1 [[1909.01820](#)].
- [61] V. K. Tkachenko, *On vortex lattices*, *Sov. Phys. JETP* **22** (1965) 1282.
- [62] V. K. Tkachenko, *Stability of vortex lattices*, *Sov. Phys. JETP* **23** (1966) 1049.
- [63] V. K. Tkachenko, *Elasticity of vortex lattices*, *Sov. Phys. JETP* **29** (1969) 945.
- [64] Y.-H. Du, S. Moroz, D. X. Nguyen and D. T. Son, *Noncommutative Field Theory of the Tkachenko Mode: Symmetries and Decay Rate*, [2212.08671](#).
- [65] H. Watanabe and H. Murayama, *Redundancies in Nambu-Goldstone Bosons*, *Phys. Rev. Lett.* **110** (2013) 181601 [[1302.4800](#)].
- [66] B. Sutherland, *Some Exact Results for One-Dimensional Models of Solids*, *Phys. Rev. A* **8** (1973) 2514.
- [67] M. Nitta, *Moduli space of global symmetry in $N=1$ supersymmetric theories and the quasiNambu-Goldstone bosons*, *Int. J. Mod. Phys. A* **14** (1999) 2397 [[hep-th/9805038](#)].
- [68] M. Nitta and D. A. Takahashi, *Quasi-Nambu-Goldstone modes in nonrelativistic systems*, *Phys. Rev. D* **91** (2015) 025018 [[1410.2391](#)].
- [69] H. Li, D. Kusnezov and F. Iachello, *Group theoretical properties and band structure of the lamé hamiltonian*, *Journal of Physics A: Mathematical and General* **33** (2000) 6413.
- [70] M. Kobayashi and M. Nitta, *Nonrelativistic Nambu-Goldstone Modes Associated with Spontaneously Broken Space-Time and Internal Symmetries*, *Phys. Rev. Lett.* **113** (2014) 120403 [[1402.6826](#)].
- [71] M. Kobayashi and M. Nitta, *Nonrelativistic Nambu-Goldstone modes propagating along a Skyrmion line*, *Phys. Rev. D* **90** (2014) 025010 [[1403.4031](#)].
- [72] H. Watanabe and H. Murayama, *Nambu-Goldstone bosons with fractional-power dispersion relations*, *Phys. Rev. D* **89** (2014) 101701 [[1403.3365](#)].
- [73] D. A. Takahashi, M. Kobayashi and M. Nitta, *Nambu-Goldstone Modes Propagating along Topological Defects: Kelvin and Ripple Modes from Small to Large Systems*, *Phys. Rev. B* **91** (2015) 184501 [[1501.01874](#)].

- [74] N. Yamamoto, *Axion electrodynamics and nonrelativistic photons in nuclear and quark matter*, *Phys. Rev. D* **93** (2016) 085036 [[1512.05668](#)].
- [75] I. Dzyaloshinskii, *A Thermodynamic Theory of ‘Weak’ Ferromagnetism of Antiferromagnetics*, *J. Phys. Chem. Solids* **4** (1958) 241.
- [76] T. Moriya, *Anisotropic Superexchange Interaction and Weak Ferromagnetism*, *Phys. Rev.* **120** (1960) 91.
- [77] Y. Togawa, T. Koyama, K. Takayanagi, S. Mori, Y. Kousaka, J. Akimitsu et al., *Chiral magnetic soliton lattice on a chiral helimagnet*, *Phys. Rev. Lett.* **108** (2012) 107202.
- [78] Y. Togawa, Y. Kousaka, K. Inoue and J.-I. Kishine, *Symmetry, structure, and dynamics of monoaxial chiral magnets*, *J. Phys. Soc. Jpn.* **85** (2016) 112001.
- [79] J.-I. Kishine and A. Ovchinnikov, *Chapter one - theory of monoaxial chiral helimagnet*, vol. 66 of *Solid State Physics*, pp. 1–130, Academic Press, (2015), [DOI](#).
- [80] A. A. Tereshchenko, A. S. Ovchinnikov, I. Proskurin, E. V. Sinitsyn and J.-I. Kishine, *Theory of magnetoelastic resonance in a monoaxial chiral helimagnet*, *Phys. Rev. B* **97** (2018) 184303.
- [81] J. Chovan, N. Papanicolaou and S. Komineas, *Intermediate phase in the spiral antiferromagnet $\text{Ba}_2\text{CuGe}_2\text{O}_7$* , *Phys. Rev. B* **65** (2002) 064433.
- [82] C. Ross, N. Sakai and M. Nitta, *Exact ground states and domain walls in one dimensional chiral magnets*, *JHEP* **12** (2021) 163 [[2012.08800](#)].
- [83] Y. Amari and M. Nitta, *Chiral magnets from string theory*, *JHEP* **11** (2023) 212 [[2307.11113](#)].
- [84] C. Ross and M. Nitta, *Domain-wall skyrmions in chiral magnets*, *Phys. Rev. B* **107** (2023) 024422 [[2205.11417](#)].
- [85] Y. Amari, C. Ross and M. Nitta, *Domain-wall skyrmion chain and domain-wall bimerons in chiral magnets*, [2311.05174](#).
- [86] M. Kobayashi, E. Nakano and M. Nitta, *Color Magnetism in Non-Abelian Vortex Matter*, *JHEP* **06** (2014) 130 [[1311.2399](#)].